Geophys. J. Int. (2004) **156,** 377–408 doi: 10.1111/j.1365-246X.2003.02132.x

Systematic variation in the depths of slabs beneath arc volcanoes

P. England,[1] R. Engdahl[2] and W. Thatcher[3]

[1] *Department of Earth Sciences, Oxford University, Parks Road, Oxford* OX1 3PR, *UK*
[2] *Department of Physics, University of Colorado at Boulder, Campus Box* 390, *Boulder,* CO 80309-390, *USA*
[3] *US Geological Survey,* MS 977, 345 *Middlebrows Road, Melon Park,* CA 94025*, USA*

Accepted 2003 September 23. Received 2003 August 15; in original form 2002 August 15

SUMMARY

The depths to the tops of the zones of intermediate-depth seismicity beneath arc volcanoes are determined using the hypocentral locations of Engdahl *et al*. These depths are constant, to within a few kilometres, within individual arc segments, but differ by tens of kilometres from one arc segment to another. The range in depths is from 65 km to 130 km, inconsistent with the common belief that the volcanoes directly overlie the places where the slabs reach a critical depth that is roughly constant for all arcs. The depth to the top of the intermediate-depth seismicity beneath volcanoes correlates neither with age of the descending ocean floor nor with the thermal parameter of the slab. This depth does, however, exhibit an inverse correlation with the descent speed of the subducting plate, which is the controlling factor both for the thermal structure of the wedge of mantle above the slab and for the temperature at the top of the slab. We interpret this result as indicating that the location of arc volcanoes is controlled by a process that depends critically upon the temperature at the top of the slab, or in the wedge of mantle, immediately below the volcanic arc.

Key words: island arcs, seismicity, volcanoes.

1 INTRODUCTION

It is generally accepted that the volcanic front at subduction zones lies above the place where the slab has reached a critical depth that does not vary much from arc to arc. Several studies have attempted to determine this depth (e.g. Gill 1981; Bevis & Isacks 1984; Jarrard 1986; Tatsumi & Eggins 1995; Tatsumi 1986), yielding estimates between about 110 km (108 ± 14 km and 112 ± 19 km Tatsumi & Eggins 1995; Tatsumi 1986) and 125 km (124 ± 38 km Gill 1981). This range of depths is quite small, indeed the different estimates are statistically indistinguishable from one another, supporting the general acceptance of a constant depth to the slab beneath the volcanic front. This paper, however, is motivated by a simple question: is the depth to the slab beneath the volcanic fronts indeed approximately constant, or does the scatter of depths in the estimates quoted above arise from systematic variation from one arc to another? We address this question using the information contained in precise earthquake hypocentral locations (Engdahl *et al.* 1998) to determine the vertical separation between the intermediate-depth seismicity and the volcanic arcs, finding that this separation varies systematically with the descent speed of the slab.

2 DEPTH OF THE SLAB BENEATH ARC VOLCANOES

A definition sketch for the terms we use to describe the geometry of subduction zones is shown in Fig. 1. The depth to the slab is not usually directly measurable, especially beneath the arc volcanoes. We employ as a proxy the depth to the top of the zone of intermediate-depth seismicity beneath the volcanoes, which we determine from cross-sections of hypocentres perpendicular to the arcs. In all the arcs studied, the focal mechanisms of earthquakes occurring beneath the volcanoes exhibit the down-dip extension or compression that is characteristic of internal deformation of the slab (Isaacs & Molnar 1971), and not the shallow thrust-faulting mechanisms that characterize the plate boundary. It appears, however, that the top of the intermediate-depth seismicity beneath the volcanic arcs is continuous with the surface defined by the plane of shallow thrust-faulting on the plate boundary (e.g. Abers 1992; Igarishi *et al.* 2001) and it has been shown in some places that the intermediate-depth earthquakes beneath volcanoes lie a few kilometres below a sharp interface marking the top of the slab (e.g. Engdahl & Gubbins 1987; Helffrich & Abers 1997; Zhao *et al.* 1994, 1997). We therefore assume, in what follows, that the offset between the top of the intermediate-depth seismicity and the top of the slab is no more than a few kilometres.

2.1 Identification of volcanic arcs

The locations of volcanoes are taken from the compilation of Holocene volcanoes by the Smithsonian Institution Global Volcanism Project (Siebert & Simkin 2002). Individual segments of arcs were identified by visual inspection. The ends of segments are usually clearly defined by changes in the strike of the volcanic front. Often, these changes in strike correspond to the locations of fracture

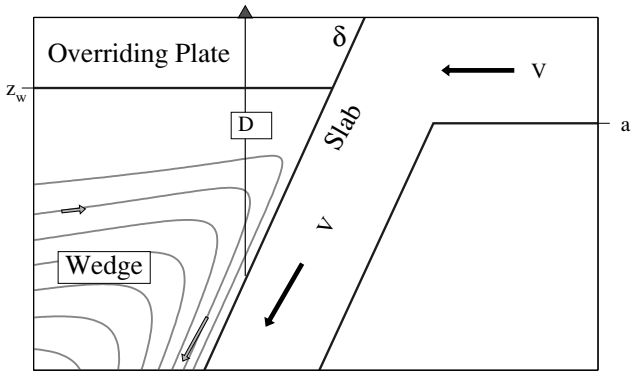

Figure 1. Idealized sketch of a subduction zone, illustrating terminology and parameters used in the paper. Two plates converge at a speed V, measured perpendicular to the trend of the island arc. A slab, of thickness a, dips at an angle, δ, beneath the overriding plate. The relative motion between slab and overriding plate generates circulation in the wedge of mantle between them, which is here depicted as though it conformed to the flow of a Newtonian fluid with velocity equal to zero on the top of the wedge, and equal to the velocity of the slab on the base of the wedge (the 'corner flow' of M^{c}Kenzie (1969)). The base of the overriding plate, and thus the wedge corner, are at depth z_w, and the boundary between the two plates lies on the top of the slab, between the surface and the wedge corner at depth z_w. The material of the wedge follows stream lines, shown as curved lines; illustrative arrows show the relative magnitudes of the velocity in different parts of the wedge. A volcano, depicted by the triangle, lies at a distance D above the top of the slab. In this paper, the top of the intermediate-depth seismicity is taken as a proxy for the top of the slab (see text).

zones or other prominent features in the subducting plate. In several cases we have divided arcs that are commonly treated as units (most notably the Aleutian and Kuriles arcs) into two or more segments; as is shown in Table 1, these separate segments are characterized by different subduction parameters, principally dip or convergence rate.

Our aim is not only to determine as precisely as possible the depths to the top of the zone of intermediate-depth seismicity, but also to investigate whether there is any systematic variation in these depths with parameters such as the speed of subduction, or the dip of the slab. We therefore excluded some volcanic arcs from this study for one or more of the following reasons. In some cases the volcanoes are distributed over a broad region, rather than being confined to narrow arcs (e.g. Ecuador, Central Andes). In other cases, there are too few earthquakes to allow us to identify a clear seismic zone and thus measure a depth to its upper surface beneath the volcanoes (western North America, northernmost and southernmost South America). Finally, there are several arc segments, such as those to the north of the Australian plate and around the south of the Philippine plate, that involve small plates whose relative motions are poorly constrained. Because rates of plate motion are central to our analysis, we also exclude those arcs.

We fit small circles to the locations of volcanoes in individual arc segments by minimizing the quantity

$$\sum_n \exp\left(\frac{-\Delta_n^2}{\sigma^2}\right)$$

where Δ_n is offset of volcano n from the small circle, and σ is a small distance, chosen empirically to be 30 km. In most cases, this procedure yields small circles very similar to those obtained using routines provided with the GMT package (Wessel & Smith 1995). Where there is a difference, we prefer our solutions because tests suggested that our procedure is less sensitive to leverage from

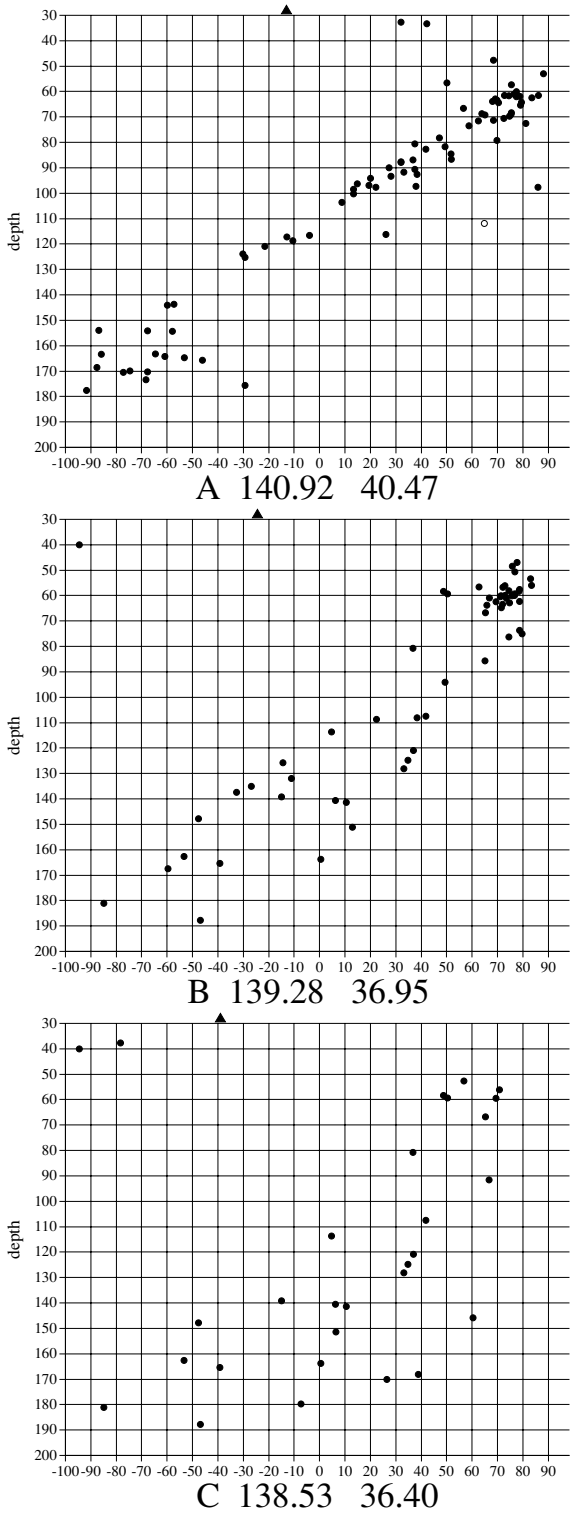

Figure 2. Cross-sections through the seismicity beneath three volcanoes in the Japanese arc, whose locations are given by the longitudes and latitudes beneath each plot. Dots show the locations of earthquake hypocentres from the catalogue of Engdahl *et al.* (1998), with the horizontal position expressed as an offset from the best-fitting small circle to the volcanic arc (see text). The solid triangles shows the offset of the individual volcanoes from that small circle. The labels A, B, and C correspond to qualities of cross-section, as discussed in the text. Picks of the depth to the top of the intermediate-depth seismicity beneath individual volcanoes, read from plots of quality A or B, are depicted on the composite cross-sections of Figs 3 to 27.

Table 1. Parameters of volcanic arcs.

Name	Depth[1]	Dip δ[2]	V_r[3]	V[4]	$V \sin\delta$[5]	Age[6]	Misfit[7]	Slab Length [8]
E. Aleutians	65 ± 5	61°	67 ± 1	65 ± 1	57 ± 1	60	6	370
C. Aleutians	80 ± 5	61°	70 ± 1	61 ± 2	54 ± 2	55	4	370
N. Kuriles	80 ± 7	49°	79 ± 1	79 ± 1	60 ± 1	120	14	890
E. Alaska Pen.	85 ± 5	57°	58 ± 2	56 ± 2	47 ± 2	46	8	650
W. Alaska Pen.	95 ± 5	50°	63 ± 2	63 ± 2	49 ± 2	46	6	530
Kamchatka	95 ± 5	54°	77 ± 2	76 ± 2	62 ± 3	90	7	860
Kermadec	95 ± 5	65°	61 ± 2	54 ± 7	49 ± 7	110	10	640
Guatemala	100 ± 5	55°	67 ± 2	67 ± 3	55 ± 3	25	6	280
N. Japan	100 ± 5	34°	92 ± 2	88 ± 3	49 ± 3	124	10	1480
S. Kuriles	100 ± 10	48°	81 ± 1	71 ± 4	52 ± 3	120	9	890
S. Sumatra	100 ± 8	56°	69 ± 1	61 ± 6	51 ± 5	80	8	380
Java	100 ± 12	40°	73 ± 1	72 ± 1	46 ± 1	130	17	870
W. Aleutians	105 ± 6	61°	72 ± 1	44 ± 6	39 ± 6	60	2	225
Ryukyus	105 ± 5	55°	52 ± 4^a	49 ± 6	40 ± 2	47	5	440
Tonga	110 ± 6	47°	78 ± 5	74 ± 6	54 ± 4	120	5	940
C. Chile	110 ± 5	30°	80 ± 1	67 ± 1	33 ± 1	34	9	730
New Zealand	110 ± 5	50°	46 ± 3	36 ± 3	27 ± 2	100	6	540
Marianas	115 ± 10	75°	37 ± 4^a	27 ± 5	26 ± 8	140	2	860
S. Peru/N. Chile	115 ± 5	35°	78 ± 1	68 ± 10	30 ± 5	50	7	1040
N. Sumatra	115 ± 5	37°	66 ± 1	47 ± 6	28 ± 5	50	7	380
West Indies	115 ± 5	47°	20 ± 1^b	19 ± 2	14 ± 1	70	2	410
Bonin	120 ± 8	42°	44 ± 2^a	30 ± 13	20 ± 9	140	5	860
Aegean	125 ± 3	43°	55 ± 7^c	43 ± 16	30 ± 11	120	2	340
Izu	130 ± 6	47°	55 ± 4^a	51 ± 4	37 ± 4	140	8	860

[1] Average depth to top of intermediate earthquakes below volcanoes of the arc, in kilometres, read from Figs 3 to 27. The uncertainties listed reflect ranges of adjusted picks of depth shown by the histograms in those figures, not the uncertainties discussed in Section 2.2.

[2] Average dip of the seismic zone between depth of 80 km, and 400 km or the termination of intermediate-depth seismicity, whichever is the more shallow. The uncertainty in these dips is taken to be 2.5°, throughout.

[3] Average rate of relative motion between the two plates bordering the arc, from the angular velocities of DeMets *et al.* (1994), in millimetres per year. Uncertainties represent the range in V along the arc segment. See text for rates of backarc spreading (Section 3.1) and the explanation for not using them to calculate V (Section 3.2). Rates for arcs bordering the Philippine plate (^{a}) are calculated from the angular velocities of Seno *et al.* (1993) for the Philippine plate. The rate for the Lesser Antilles (^{b}) is calculated from the angular velocity of DeMets *et al.* (2000). The rate for the Aegean (^{c}) is calculated from the Aegean-Eurasia angular velocity of Le Pichon *et al.* (1995) and the Africa-Eurasia angular velocity of DeMets *et al.* (1994).

[4] Average rate of convergence, in millimetres per year; the plate relative velocity is resolved perpendicular to the best-fitting small circle through the volcanic arc. Uncertainties represent the range in rate along the arc segment.

[5] Average of the vertical component of the subduction velocity in millimetres per year; the convergence rate is multiplied by $\sin\delta$. Uncertainties represent the range in rate along the arc segment.

[6] Average of the age of ocean floor entering the trench (Mueller *et al.* 1997).

[7] rms misfit of volcano locations to small circle (Section 2.1), in kilometres.

[8] Down-dip length of slab in kilometres (Jarrard 1986).

outliers. Table 1 shows that the greatest rms deviation of volcano location from the best-fitting small circle is 17 km and that, in all but two cases, the rms deviation is 10 km or less.

2.2 Earthquake hypocentres

We use the hypocentral catalogue of Engdahl *et al.* (1998) which, through the systematic incorporation of depth phases in hypocentral estimation, provides a significant improvement in depth resolution over previous global catalogues. Nevertheless, doubts still remain about the reliability of the locations, principally for two reasons (Engdahl *et al.* 1998). First, the depth phases are handled automatically by an algorithm that assigns reported arrivals, usually read from short-period seismograms, to phases on the basis of probability density functions. Second, strong lateral heterogeneity in wave speeds associated with subduction may introduce biases into epicentral locations.

Engdahl *et al.* (1998) (EHB) compared the focal depths obtained by their procedures against the depths obtained by the National Earthquake Information Centre through reading individual pP-P and sP-P delays from broad-band seismograms (BBD), and inverting for depth from the time differences between these phases observed at several stations. Engdahl *et al.* (1998) found a small positive bias in depth (EHB-BBD 4–5 km, range 0–10 km) between the two methods (Engdahl *et al.* 1998, Fig 10a).

There undoubtedly are systematic differences between teleseismically determined epicentres of earthquakes in subduction zones and epicentres determined from local networks, with the teleseismic locations generally being shifted arc-ward, relative to their locally-determined positions (e.g. Fujita & Sleep 1981; Engdahl *et al.* 1982; Abers 1992). These differences can be attributed to the influence of strong lateral variation in wave speed associated with the slabs. However, hypocentres determined from local networks are also subject to error, both from lateral heterogeneity in wave speed, and from

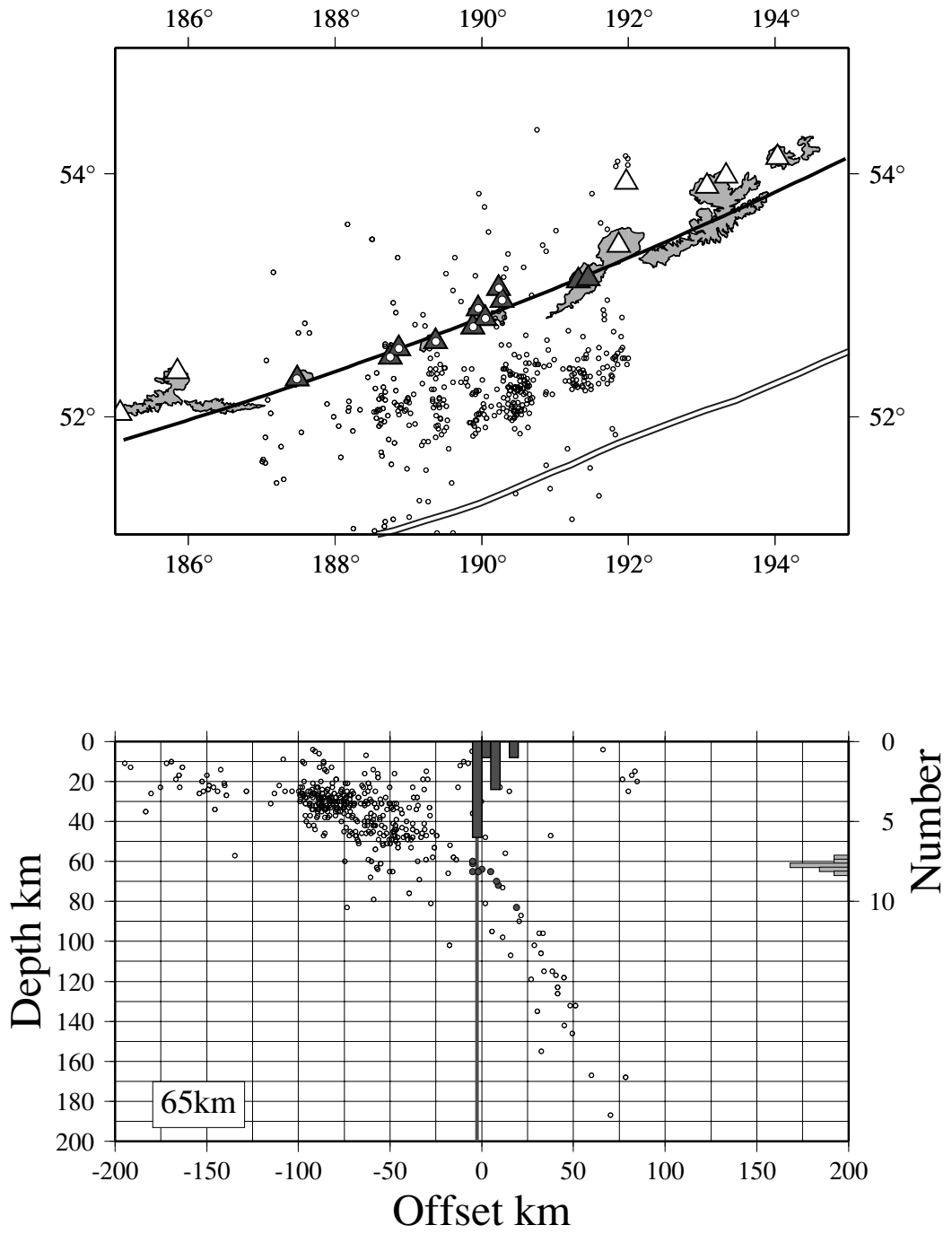

Figure 3. Map and composite cross-section of the distribution of earthquakes and volcanoes in the eastern Aleutian arc. In the upper panel, epicentres of earthquakes from the catalogue of Engdahl *et al.* (1998) are shown by open circles, and the locations of volcanoes from the Smithsonian Institution Global Volcanism Project catalogue (Siebert & Simkin 2002) by triangles. Filled triangles show volcanoes taken to belong to this segment of arc, and open dots within filled triangles denote volcanoes for which an individual pick of the depth to the top of the slab has been possible from cross-sections of quality A or B (Fig. 2, and see text). The black line shows the best-fitting small circle through the locations of the volcanoes shown by filled triangles. Double line shows the location of the trench, taken from the compilation of Mueller *et al.* (1997). In the lower panel, the hypocentres of the earthquakes shown in the upper panel are plotted with the horizontal coordinate being the offset from the small circle. Histogram on the top of this panel (scale to right) indicates the numbers of volcanoes located within 5-km bins of distance from the small circle. Vertical line indicates chosen location of the volcanic front. Larger, darker, dots indicate the locations of individual picks of the depth to the intermediate-depth seismicity. Histogram to right of panel indicates the distribution of these individual picks when corrected for the offset of individual volcanoes from the small circle (see text). The estimate of depth of the top of the intermediate-depth seismicity used in Table 1 is shown in the box at the bottom left of this panel.

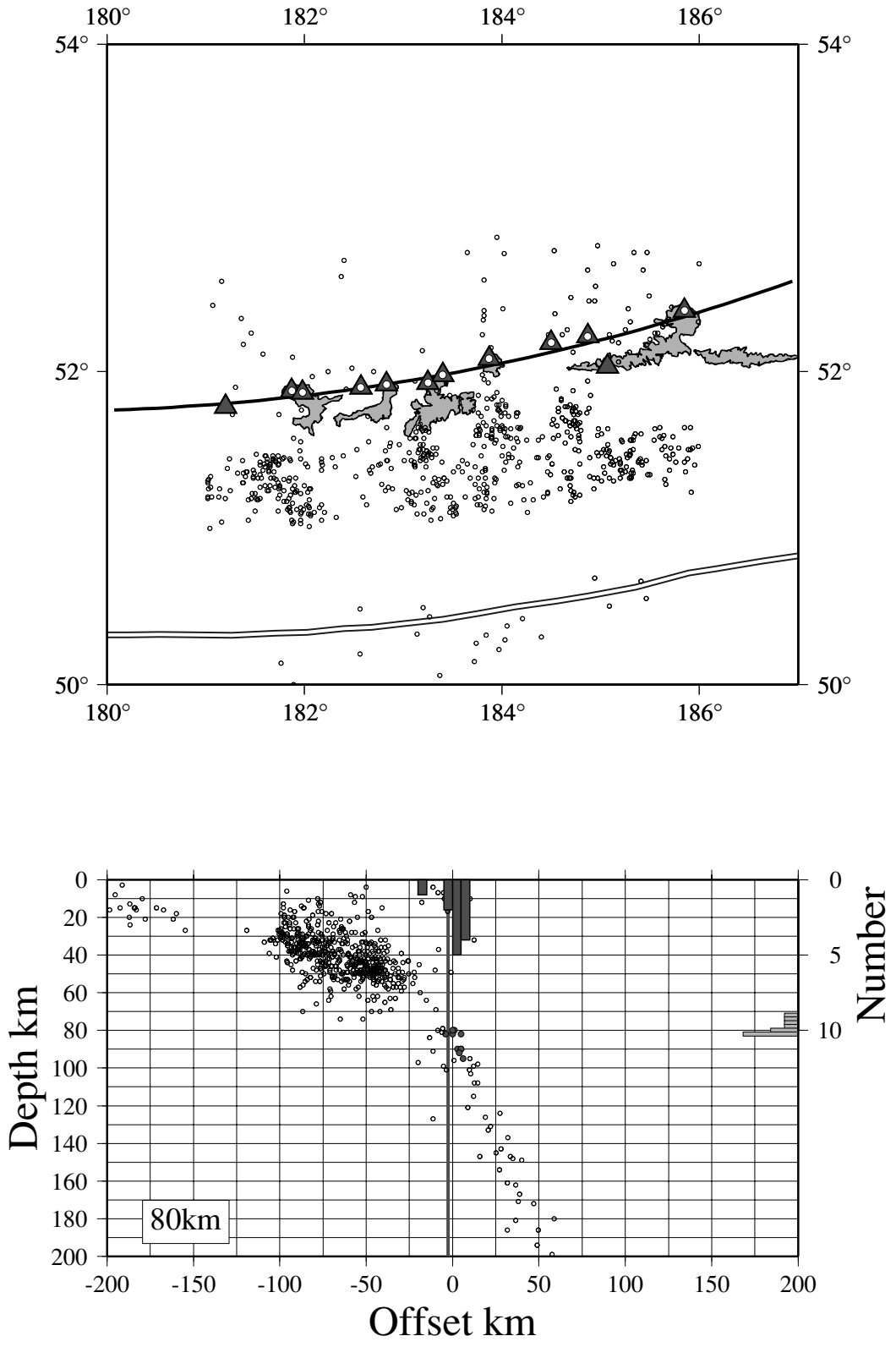

Figure 4. As Fig. 3, for the central Aleutian arc.

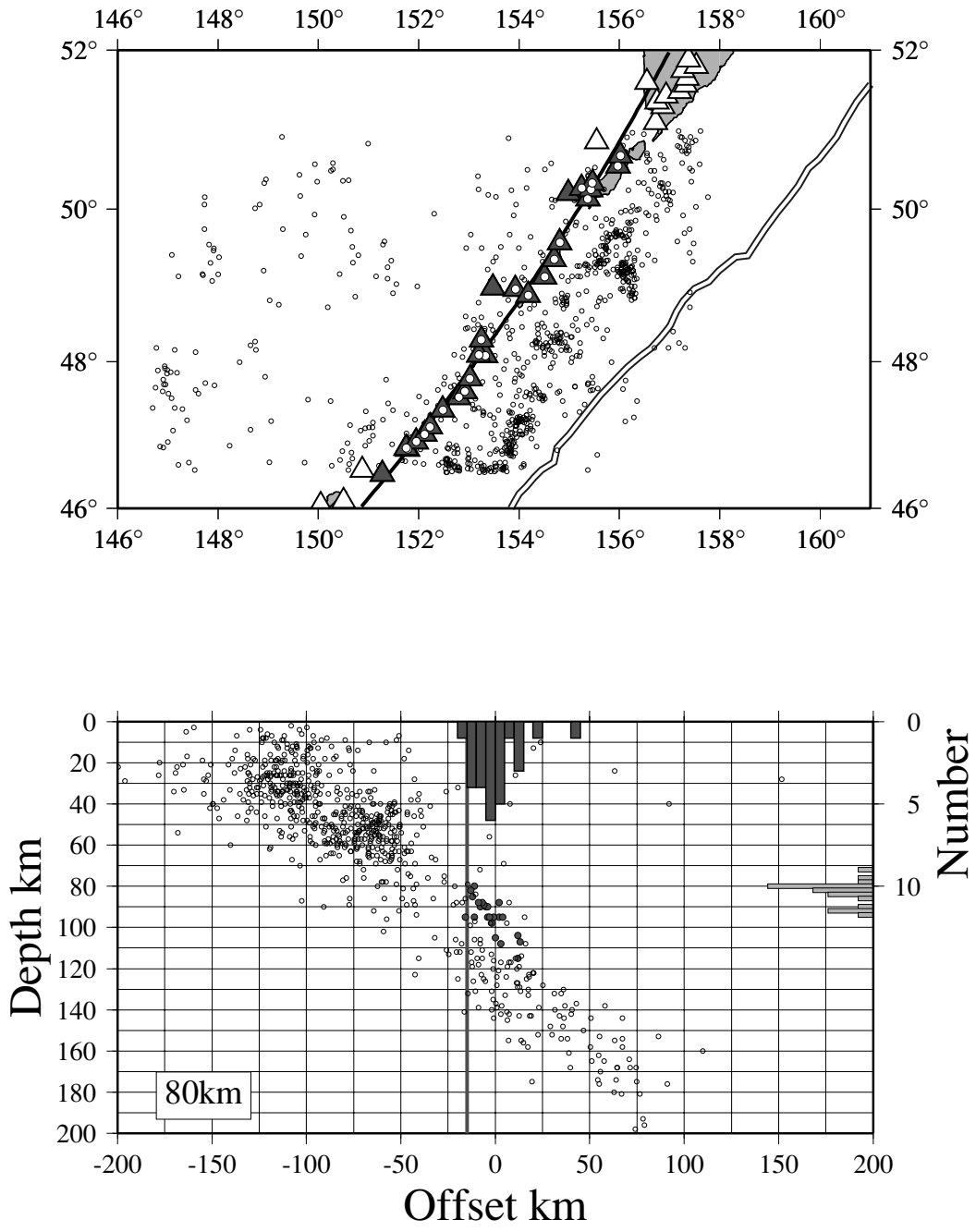

Figure 5. As Fig. 3, for the northern Kuriles arc.

unfavourable network geometry, so it is impossible to be certain of the absolute mislocation of the epicentres. Although the difference between local and teleseismic epicentres may be as great as 40–50 km for earthquakes shallower than about 50 km, this paper is concerned with the relative location of intermediate-depth seismicity and the volcanoes. At intermediate depths, the difference between local and teleseismic epicentres is usually smaller than 20 km (e.g. Engdahl *et al.* 1982, 1998). We take 20 km as a reasonable estimate of the magnitude of the systematic bias that may exist in the epicentres. Epicentral bias converts into bias in the depth of the intermediate-depth seismicity at any location through multiplication by the tangent of the dip of the slab (30–70°, Table 1). We conclude that the combined influences of mislocations in depth and epicentre may produce errors of up to 20 km in our estimates of the depth to the top of the intermediate-depth seismicity.

2.3 Depths to top of the intermediate-depth seismicity

Using hypocentral locations from the catalogue of Engdahl *et al.* (1998), we plotted cross-sections of seismicity perpendicular to the small circles fit to the volcanic arcs, and through the active volcanoes in each of the arcs investigated. The cross-sections varied in quality, as illustrated in Fig. 2 for three cross-sections through the Japanese arc. In cross-sections of the highest quality (class A, Fig. 2a), there is a well-defined and planar upper boundary to the intermediate-depth

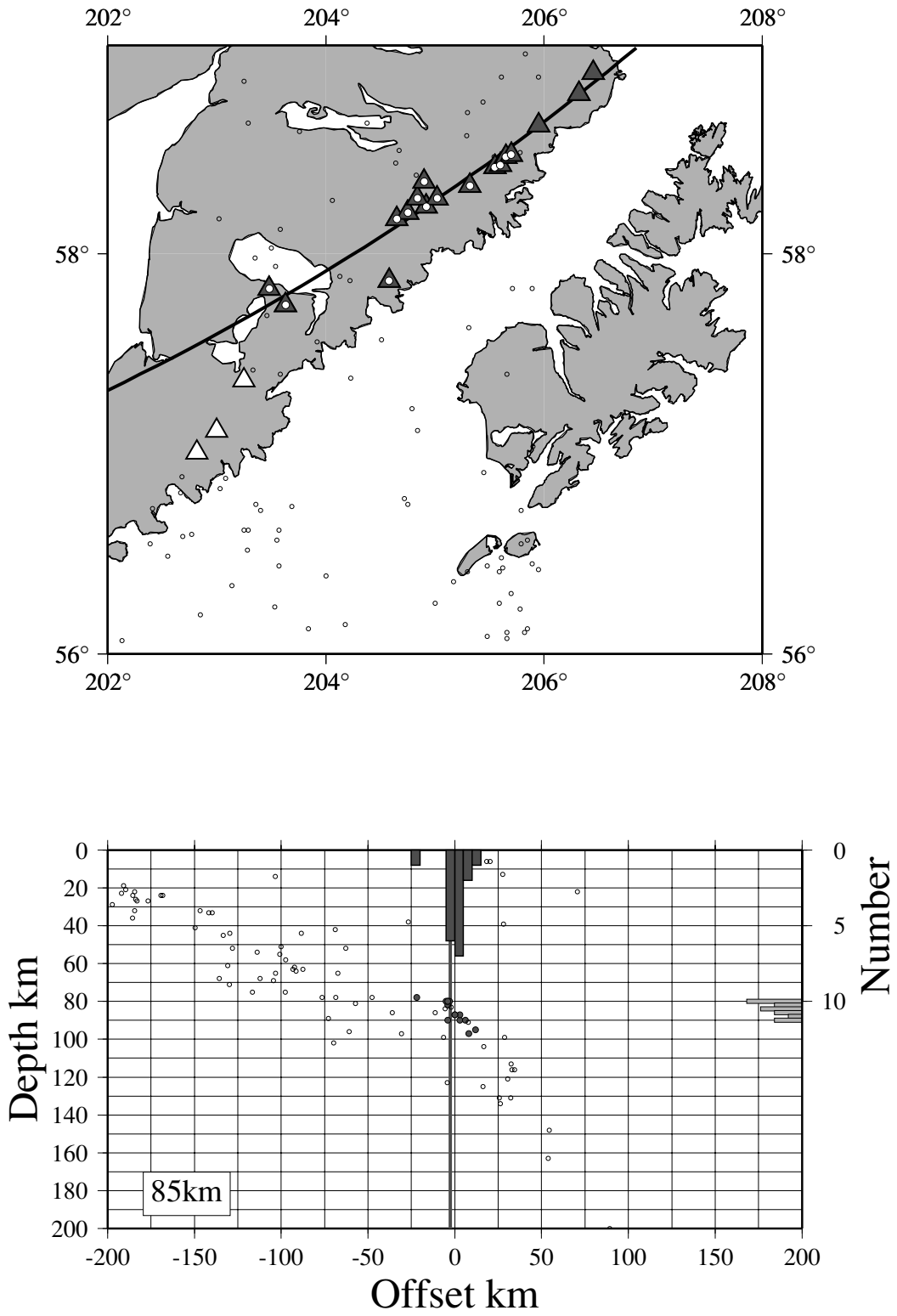

Figure 6. As Fig. 3, for the eastern Alaskan peninsula.

seismicity; at a lower level of quality (class B, Fig. 2b), the upper boundary is still discernible, but gaps in the data make its location less certain than in class A. In class C (Fig. 2c), there are too few earthquakes to identify the boundary with confidence.

For each volcano, we initially included in the cross-section all hypocentres within 100 km of the profile. If the quality of the cross-section was not at level B or better, then earthquakes within 200 km of the profile were included. Any cross-section that did not then reach

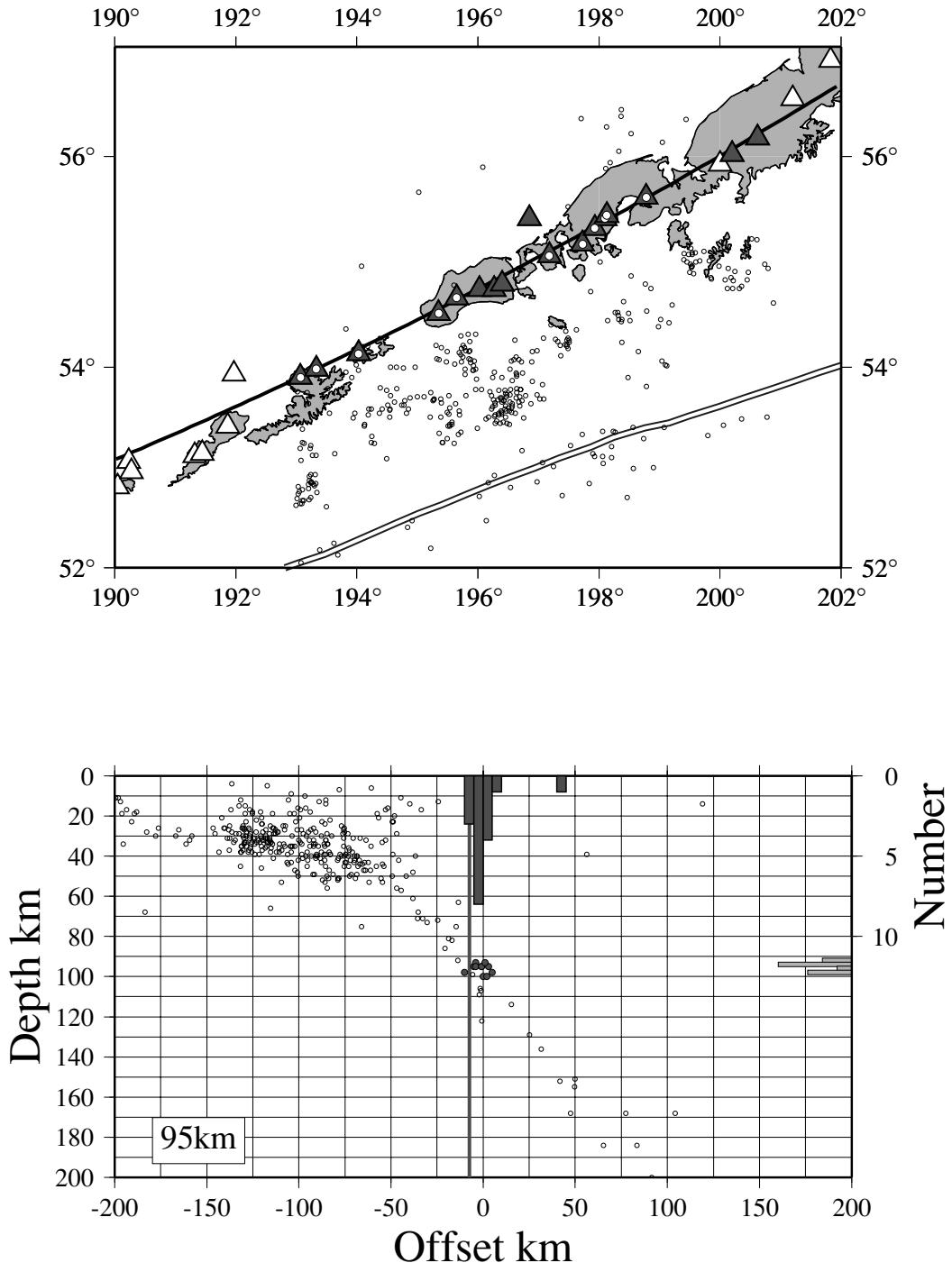

Figure 7. As Fig. 3, for the western Alaskan peninsula.

level B was not used to make an individual pick of depth. From cross-sections of quality A or B, the first and third authors independently formed estimates of the depths to the top of intermediate-depth seismicity beneath the volcanoes. These estimates agreed to within ±4 km.

It is impossible to illustrate cross-sections like Fig. 2 for each volcano, so our results are shown in summary form in Figs 3–27. These figures show cross-sections of the seismicity along the whole of each arc segment studied, with the picks of the top of seismicity from cross-sections through individual volcanoes shown as bolder symbols. The upper boundaries to the intermediate-depth seismicity in these whole-arc cross-sections mostly show cut-offs as sharp as those of the individual cross-sections of quality A, and the others are comparable with individual sections of quality B. This observation confirms the observations of many others that the zones of intermediate-depth seismicity conform closely to dipping curved surfaces whose centres of curvature match the centres of curvature of the volcanic arcs.

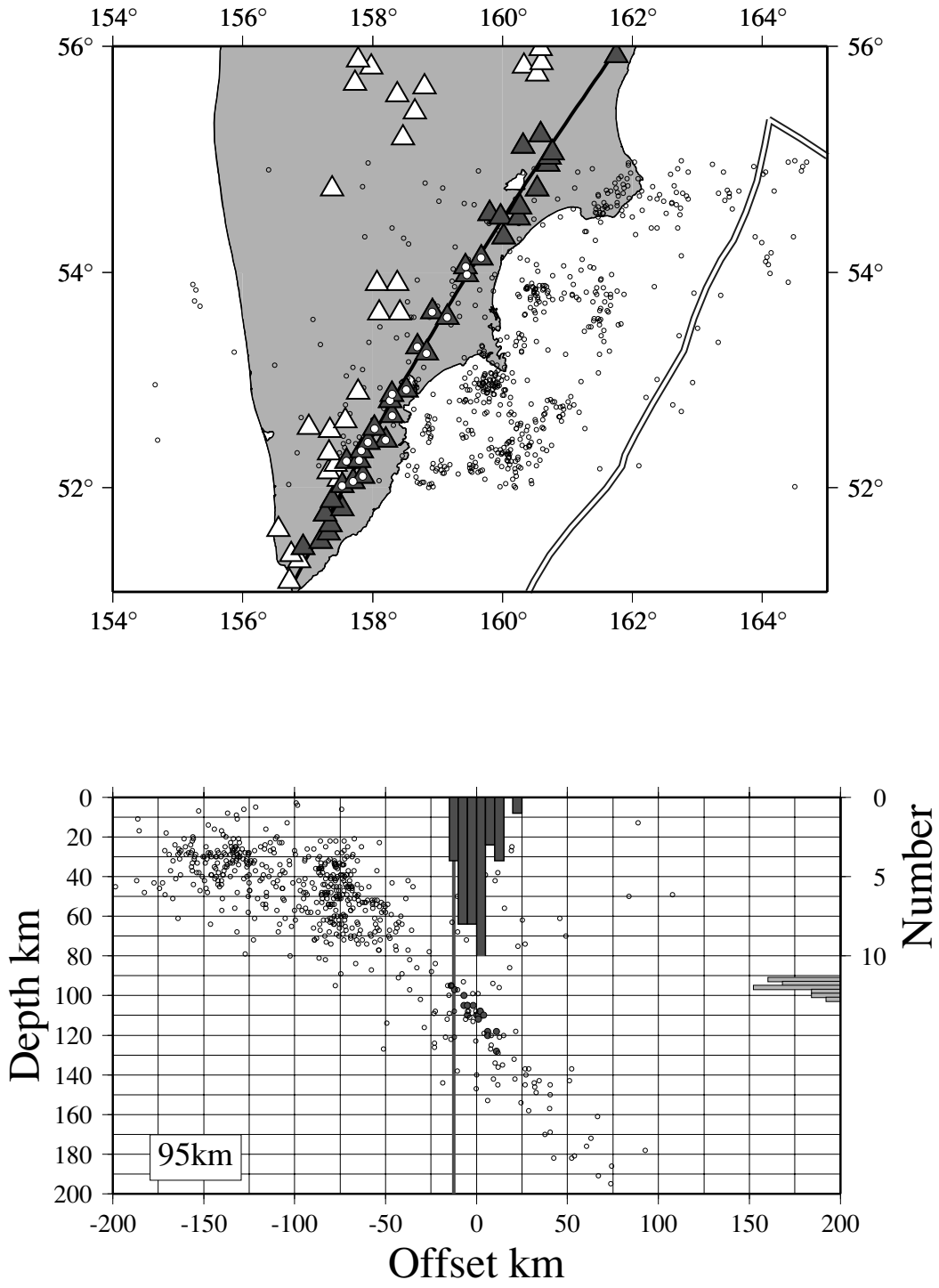

Figure 8. As Fig. 3, for the Kamchatka arc.

Each arc shows a sharp onset of volcanism at a location that can be identified to within a few kilometres (Figs 3 to 27). With the caveats discussed in Section 2, the depth of the slab beneath the volcanic front can be estimated from the upper limit of the intermediate-depth seismicity beneath the volcanic front. A second, related, estimate comes from the picks of depth to the top of the intermediate-depth seismicity made from cross-sections through the locations of individual volcanoes (discussed with reference to Fig. 2). The volcanoes lie at different distances from the volcanic front, so each pick of depth is corrected for the offset from the volcanic front by subtracting from the depth the product of the horizontal offset with the tangent of the local dip of the top of the intermediate-depth seismicity. These two estimates of the depth of the top of the intermediate-depth seismicity beneath the volcanic front agree to within a few

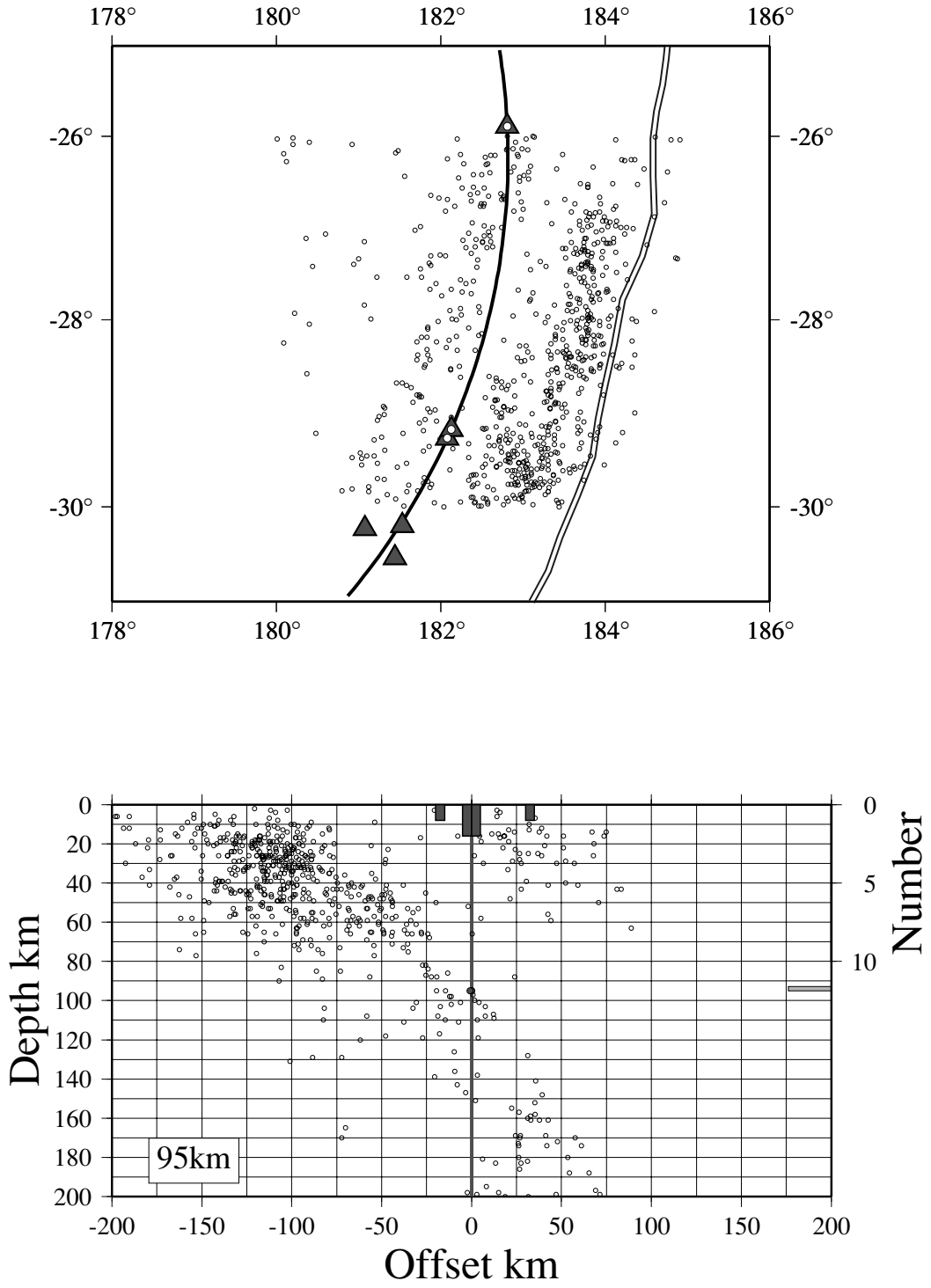

Figure 9. As Fig. 3, for the Kermadec arc.

kilometres, and are summarized in Table 1; where there is disagreement, the depth read from the whole-arc cross-sections illustrated in Figs 3 to 27 is preferred.

The distribution of depths to the tops of the intermediate-depth seismicity beneath individual volcanoes is shown in Fig. 28. The mean depth is 101 km, with a standard deviation of 16 km; these quantities are consistent with previous studies (108 ± 14 km (Tatsumi & Eggins 1995), 112 ± 19 km (Tatsumi 1986), 124 ± 38 km (Gill 1981)). Closer inspection of Figs 3 to 27 reveals, however, that this summary statistic is misleading. The depth to the top of the intermediate-depth seismicity beneath the volcanic front is uncertain by only a few kilometres for an individual arc segment, but differs by more than 60 km between arc segments. Thus the summary statistic disguises the essential feature of this distribution: the

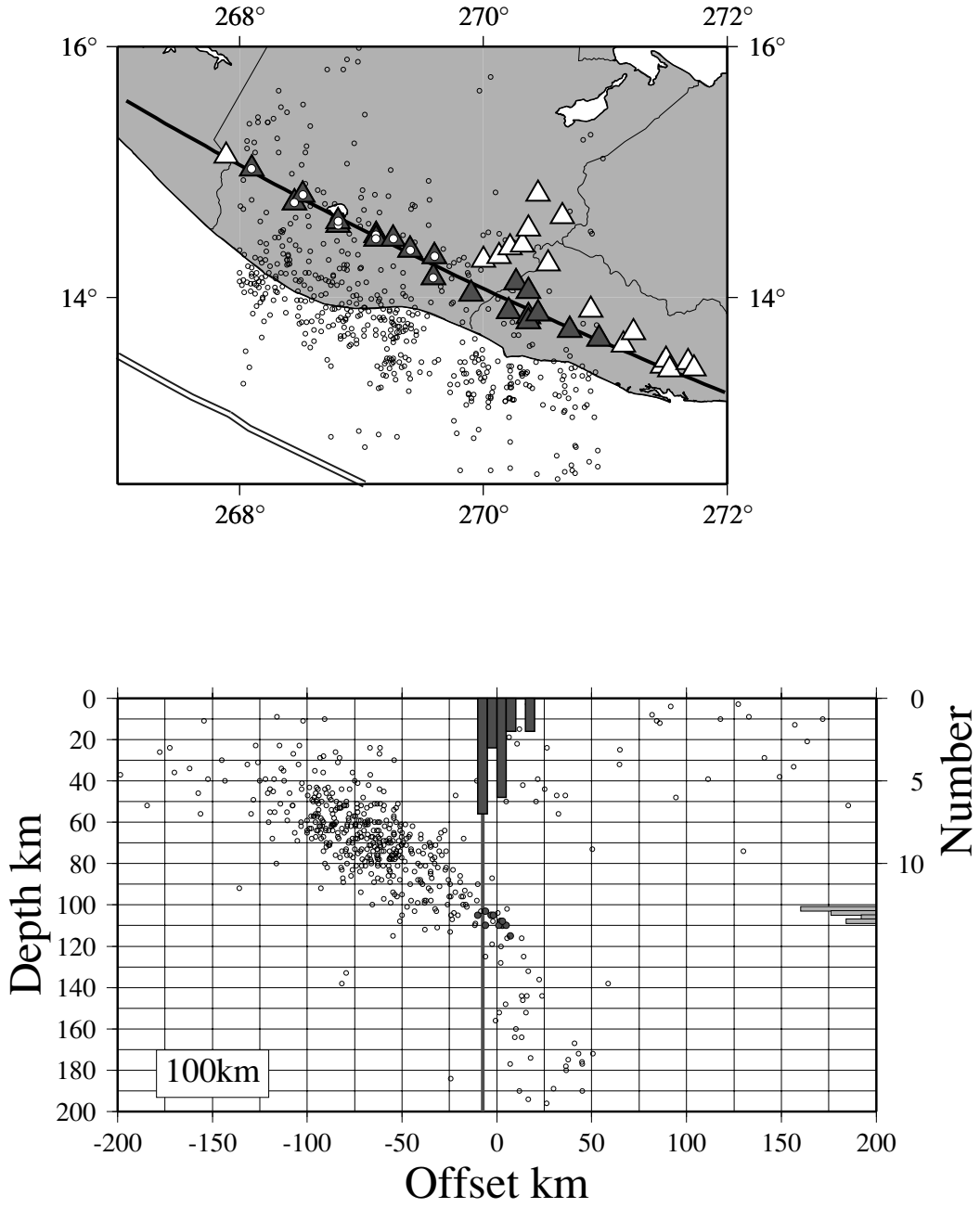

Figure 10. As Fig. 3, for Guatemala and El Salvador.

variation of depth between arcs is much greater than the uncertainty in this depth for any individual arc.

3 ANALYSIS

The observations that the volcanic arcs conform, within a few kilometres, to small circles (Table 1), and that the depth to the top of the intermediate-depth seismicity beneath the volcanic front varies little along individual arc segments (Figs 3 to 27) strongly suggest that the locations of volcanoes in island arcs are determined by processes in the subduction zone and are not greatly influenced by near-surface processes. It is therefore desirable to analyse the variation of depths to the top of the intermediate-depth seismicity in terms of parameters that are thought to govern the thermal state of the slab and upper mantle in subduction zones. We first discuss the principal parameters that have been proposed to govern the thermal structure of subduction zones and then analyse the relationship between the depth to the top of the intermediate-depth seismicity and these parameters. Finally, arguing that the temperature structure should depend only on two non-dimensional parameters (a dimensionless depth and the dip of the slab), we determine the combination of those parameters that best correlates with depth to the top of the intermediate-depth seismicity.

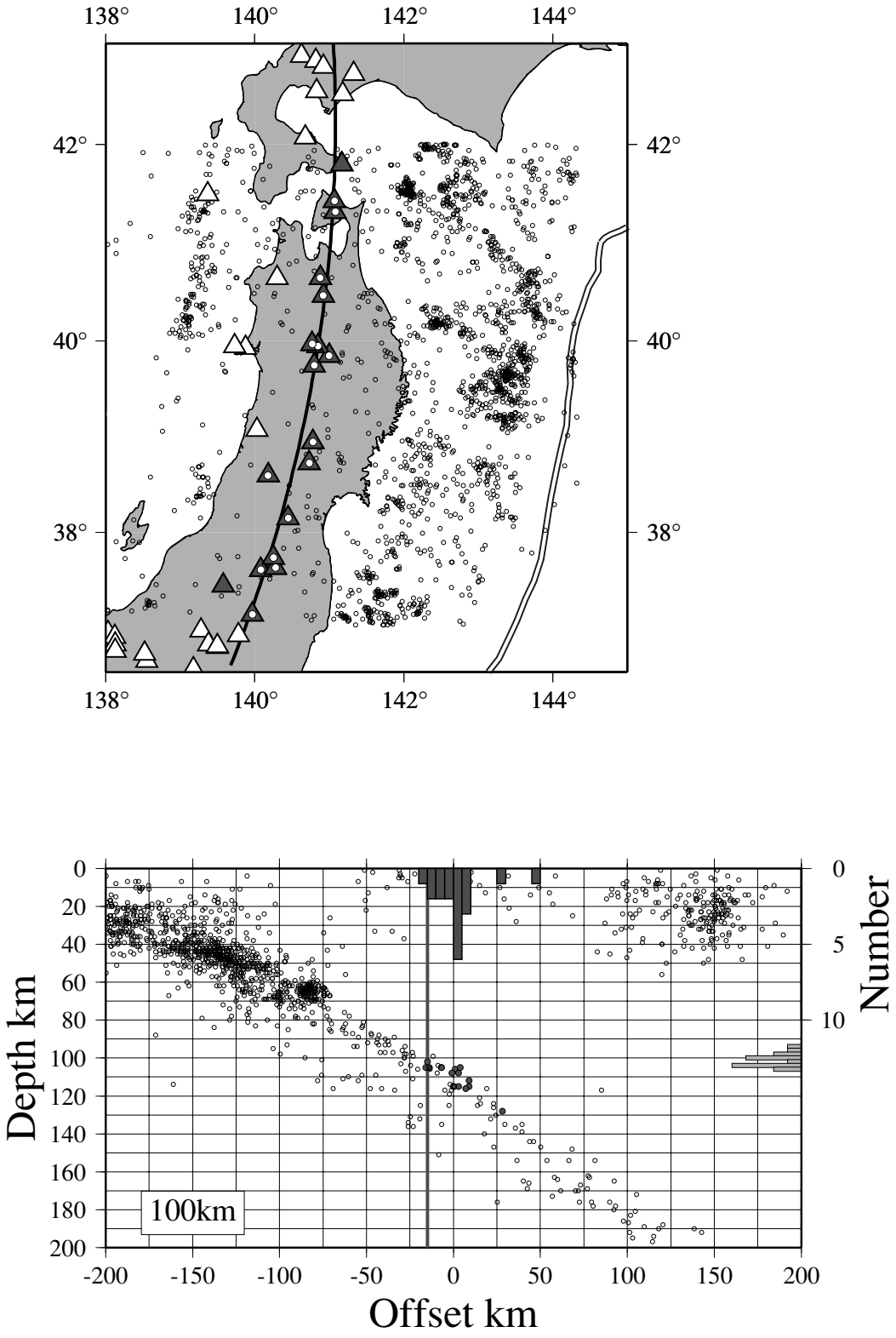

Figure 11. As Fig. 3, for the Japanese arc.

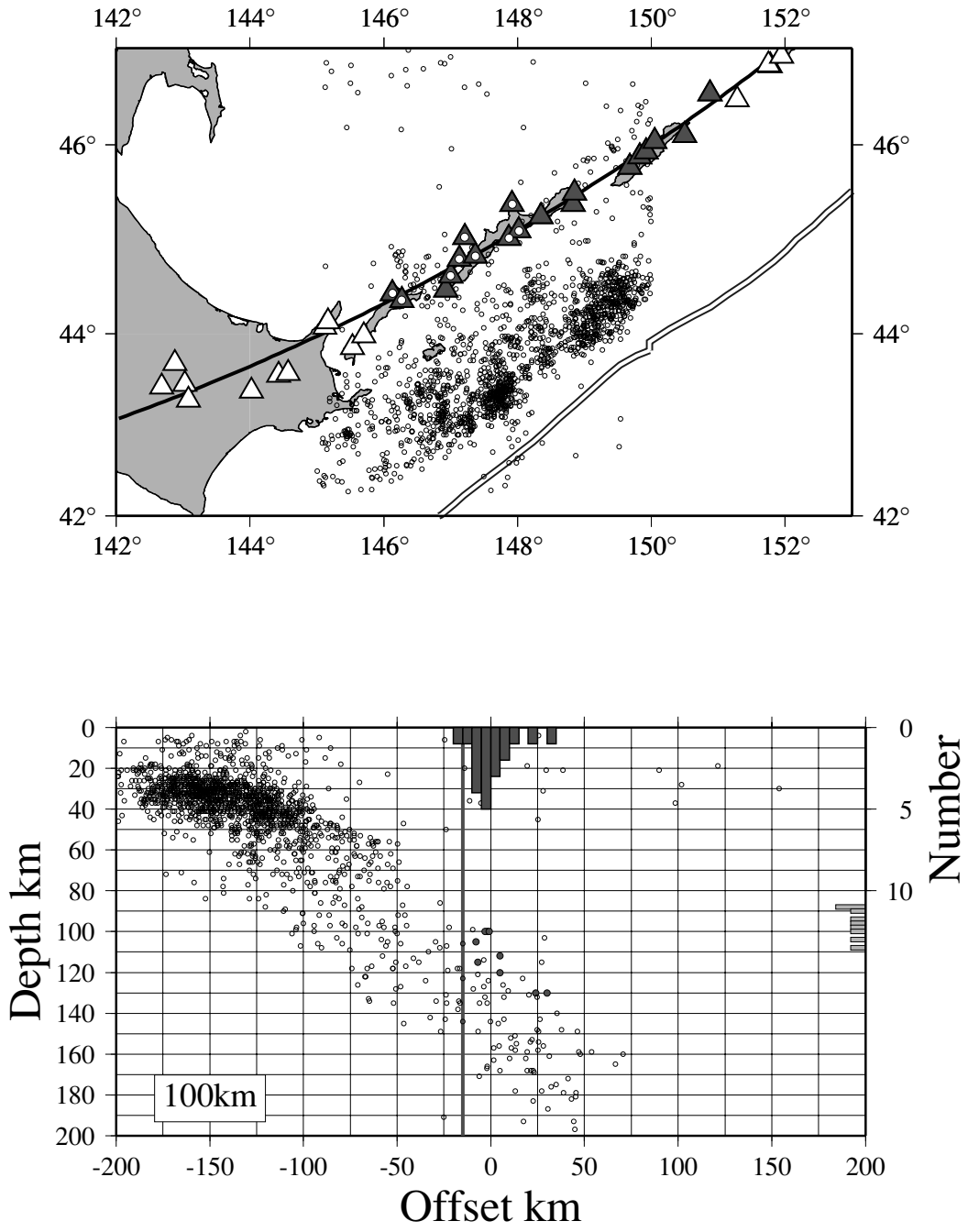

Figure 12. As Fig. 3, for the southern Kuriles arc.

3.1 Choice of parameters

We expect that any systematic variation in the vertical separation between volcanoes and slab should depend solely upon the kinematics of the subduction and upon the thermal structure of the slab, that is, upon the speed and angle of subduction and upon the age of subducting lithosphere. Table 1 lists, for each arc studied, the dip of the zone of intermediate-depth seismicity, the rate of plate relative motion, the rate of convergence (total plate relative velocity resolved perpendicular to the arc), the descent rate of the slab (convergence rate multiplied by the sine of the dip), the age of its ocean floor, and the length of the slab.

We take the age of the ocean floor beneath the volcanic front to be the same as that close to the oceanic trench, which we determined from the digital database of magnetic isochrons (Mueller *et al.* 1997). We neglect differences between the age of the slab at the surface and its age at depths around 100 km. In Fig. 29(a) we plot the depth to the top of the intermediate-depth seismicity, D (Fig. 1), against the the age of the slab, A.

The dips of the slabs are estimated by eye from the top of the intermediate-depth seismicity in each subduction zone, between a depth of 80 km, and 400 km or the maximum depth of seismicity, whichever is smaller. We choose to measure the dip over this range of depth because we expect temperatures in the wedge of mantle

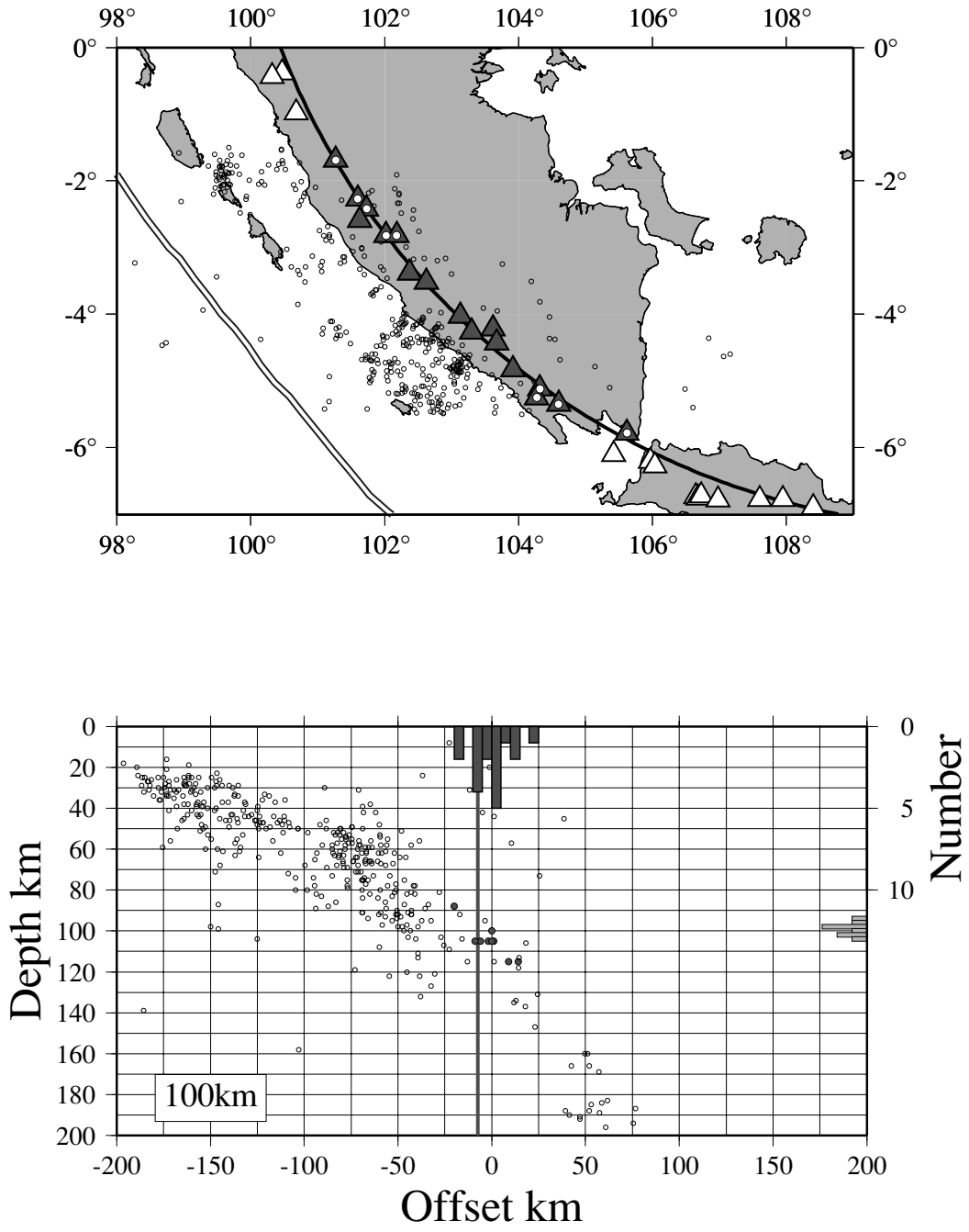

Figure 13. As Fig. 3, for the southern Sumatra arc.

between the slab and the overriding plate, and at the top of the slab, to be governed by the general circulation in the wedge and not by the detailed local configuration of the slab. For this reason we exclude the top of the slab (shallower than 80 km, where the dip often varies considerably) and depths below 400 km, where the intermediate-depth seismicity is sometimes deflected as the slab reaches the bottom of the upper mantle. Fig. 29(b) plots D against the dip, δ, of the slab.

Except for arcs involving the Caribbean and Philippine plates, relative velocities between plates are calculated from the angular velocities of DeMets *et al.* (1994). For the Caribbean-North America plate boundary, we use the angular velocity of DeMets *et al.* (2000), and for the Philippine plate, we use that of Seno *et al.* (1993). The convergence rate is taken to be the component of relative velocity perpendicular to the small circle through the arc.

Three of the arcs we analyse have significant rates of backarc spreading (Kermadec, Marianas, and Tonga). We assume full spreading rates of 54, 43, and 50 mm yr^{-1}, respectively, for these backarcs, following the arguments of Jarrard (1986), which are based on marine magnetic anomalies spanning the past 2–7 Myr; Bevis *et al.* (1995) measured rates of 160–220 mm yr^{-1} at the Tonga

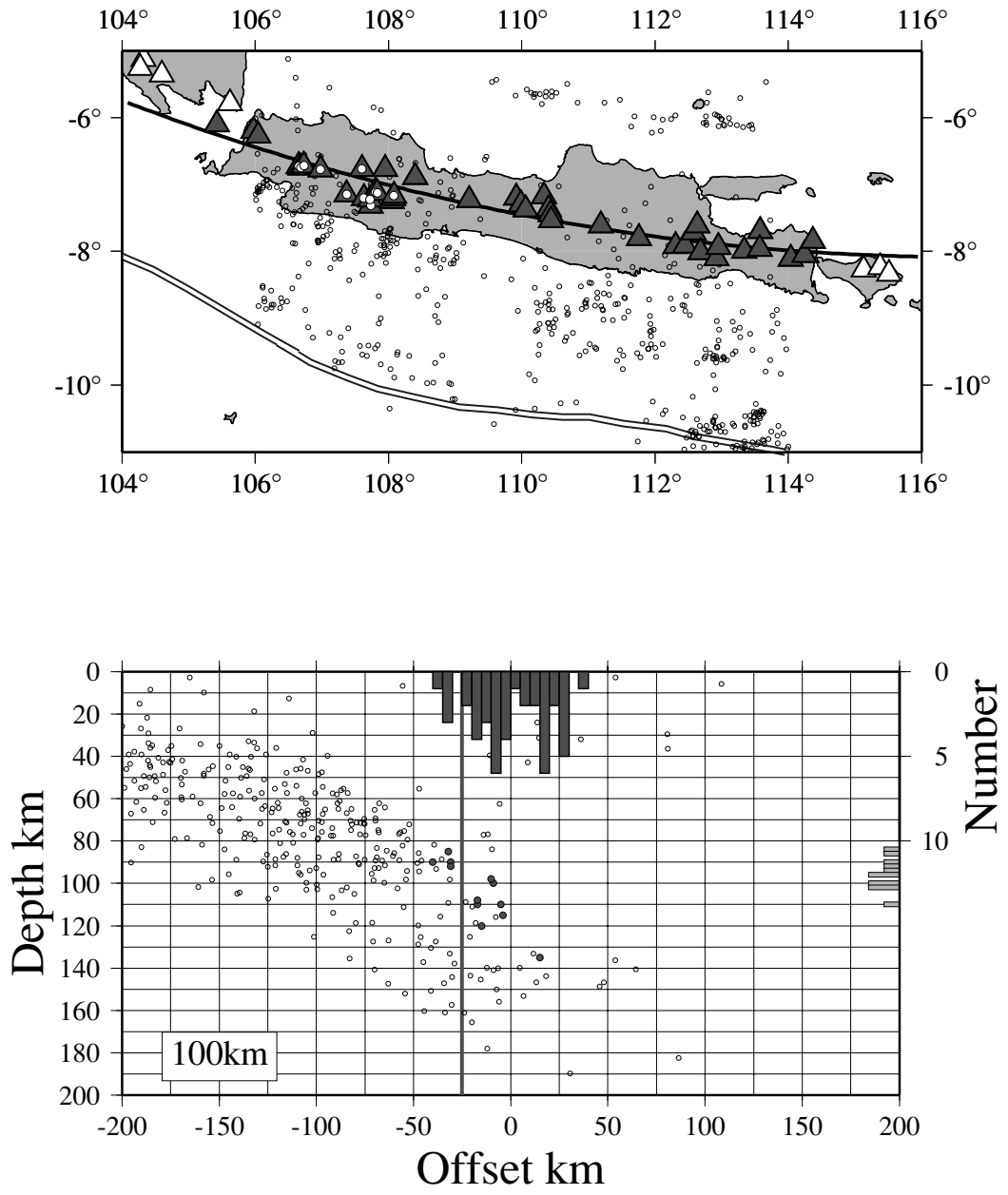

Figure 14. As Fig. 3, for Java.

arc, with a 2-yr GPS network, but we presume that the rate of spreading averaged over some millions of years is more relevant to the present thermal state of the arc. The rates of backarc spreading (and their along-arc variations) are less precisely known than plate relative velocities. Furthermore, as we discuss below (Section 3.2), the influence of backarc spreading on the thermal structure of subduction zones is poorly known, so it is unclear how to compare arcs with and without spreading. Accordingly, when a convergence rate is used in the plots below (Figs 29c–f) we represent these three arcs by two symbols: one calculated from the convergence rate between the major plates, and one with the rate of backarc spreading added in.

Fig. 29 also plots the depths against three combinations of parameters that are suggested by theoretical arguments. Temperatures beneath island arcs reflect the balance between advection of heat, by the subducting slab and the mantle circulation above it, and diffusion of heat across the steep temperature gradients induced between cold slab and hot upper mantle. Theoretical studies of the thermal structure of subduction zones therefore generally emphasize the dependence of temperature on a dimensionless distance of the form:

$$L' = \frac{UL}{\kappa}, \tag{1}$$

where L is a characteristic length, U is a characteristic speed and κ is thermal diffusivity. L' represents the ratio of the time required to diffuse heat over a distance L, L^2/κ, to the time L/U, required to carry heat the same distance at a speed U.

McKenzie (1969) investigated a problem in which the slab sinks into an upper mantle that applies a constant temperature to the surfaces of the slab and showed that the maximum down-dip distance,

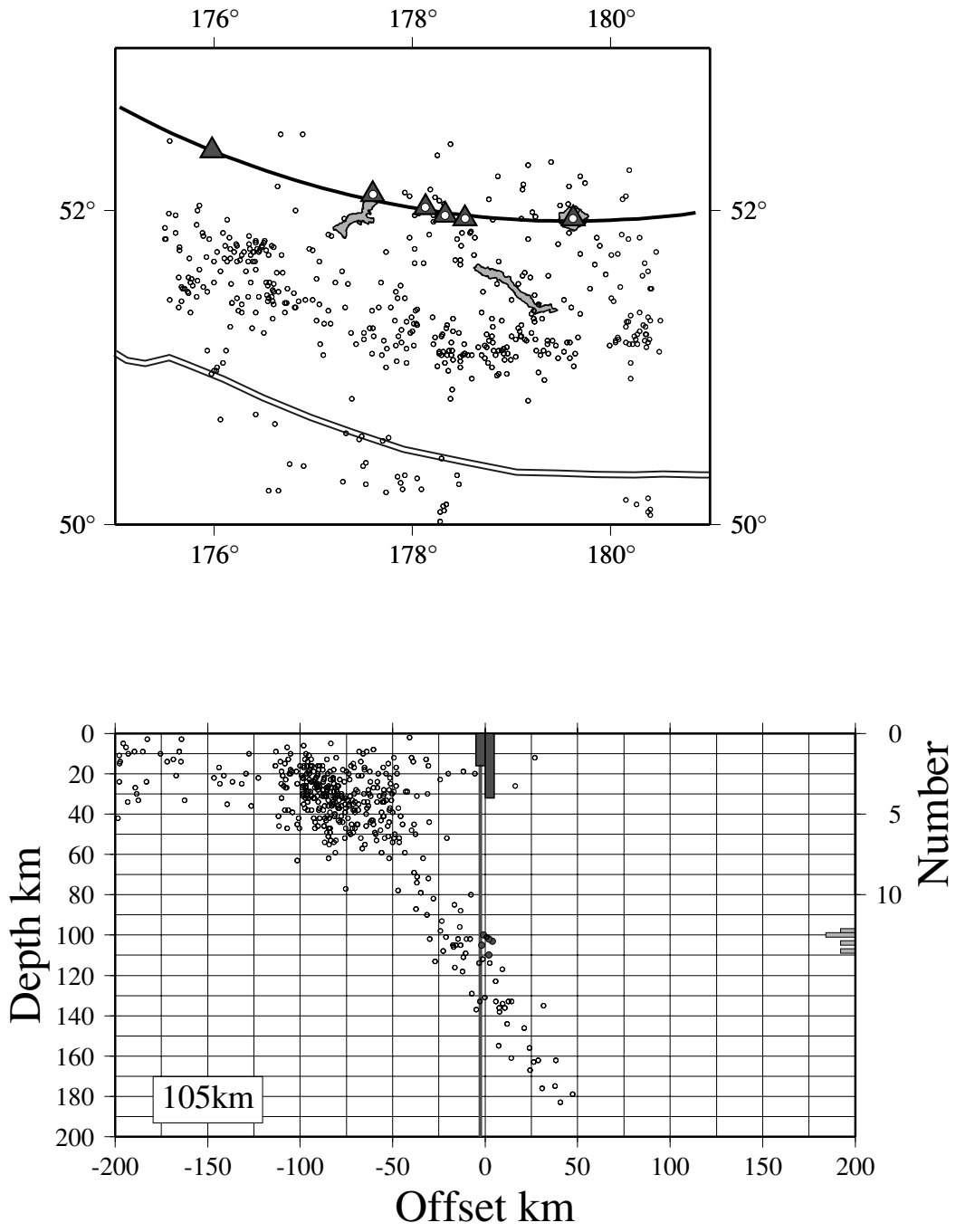

Figure 15. As Fig. 3, for the western Aleutian arc.

x_m, that an isotherm is advected by the slab is given by

$$x_{\max} = C\frac{Va^2}{\kappa}, \tag{2}$$

where C is a constant. Thus, for a slab of constant dip, δ, the maximum depth, $z_{\max}$, to which an isotherm is advected is

$$z_{\max} = x_{\max}\sin\delta = C\frac{Va^2\sin\delta}{\kappa}. \tag{3}$$

The thickness of the slab, a, is not directly measurable, but the distributions of depth of the ocean floor and of oceanic heat flux suggest that $a \sim \sqrt{\kappa A}$, where A is the age of the ocean floor (Parsons & Sclater 1978), so we may write

$$z_{\max} \sim CVA\sin\delta. \tag{4}$$

The depth to which an isotherm is advected in the interior of the slab ought, therefore, to depend upon the parameter

$$\phi = VA\sin\delta \tag{5}$$

(McKenzie 1969; Molnar *et al.* 1979). This parameter is sometimes simply called the thermal parameter of the slab (Kirby *et al.* 1991). We investigate whether the distribution of depths to the top of the intermediate-depth seismicity beneath volcanoes, D, may reflect the

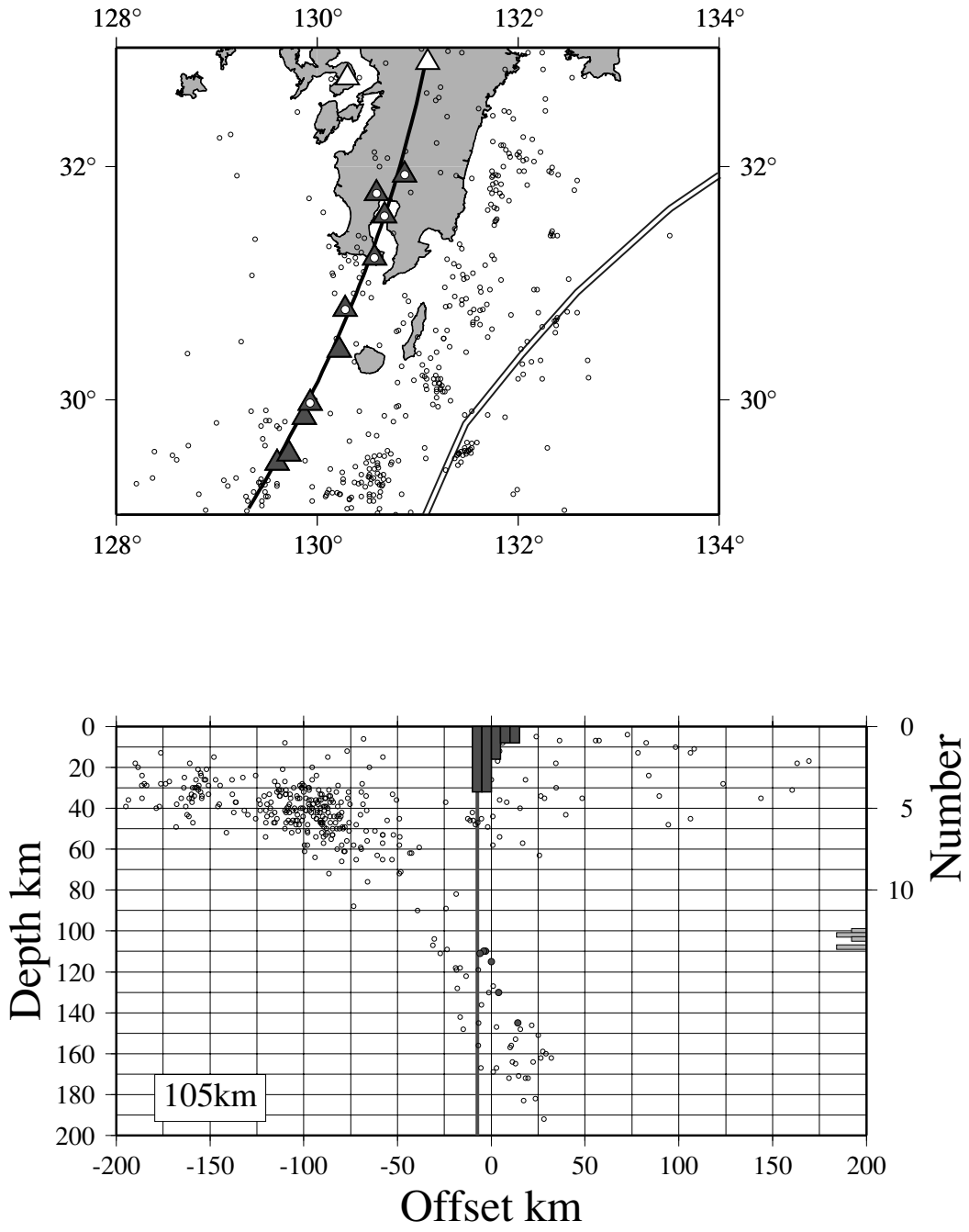

Figure 16. As Fig. 3, for the Ryukyu arc.

internal temperature structure of the slabs by plotting D against ϕ in Fig. 29(d).

The parameter ϕ measures the thermal state of the interior of the slab, but it is probable that the critical processes leading to arc volcanism are less dependent upon the internal temperature of the slab than upon temperatures at the interface between the slab and the overriding plate or between the slab and the wedge of mantle above it. Molnar & England (1990) show that, in the absence of dissipative or radioactive heating, the temperature on the interface between the two plates is given by:

$$T = \frac{Qz}{K\left(1 + b\sqrt{Vz\sin\delta/\kappa}\right)}, \tag{6}$$

where Q is heat flux to the base of the plate entering the trench, z is depth on the plate boundary, K is thermal conductivity and b is a constant, close to one. For the ranges of V and z considered here, the denominator is much greater than one, and we may write:

$$T \sim \frac{Qz}{K\sqrt{Vz\sin\delta/\kappa}}. \tag{7}$$

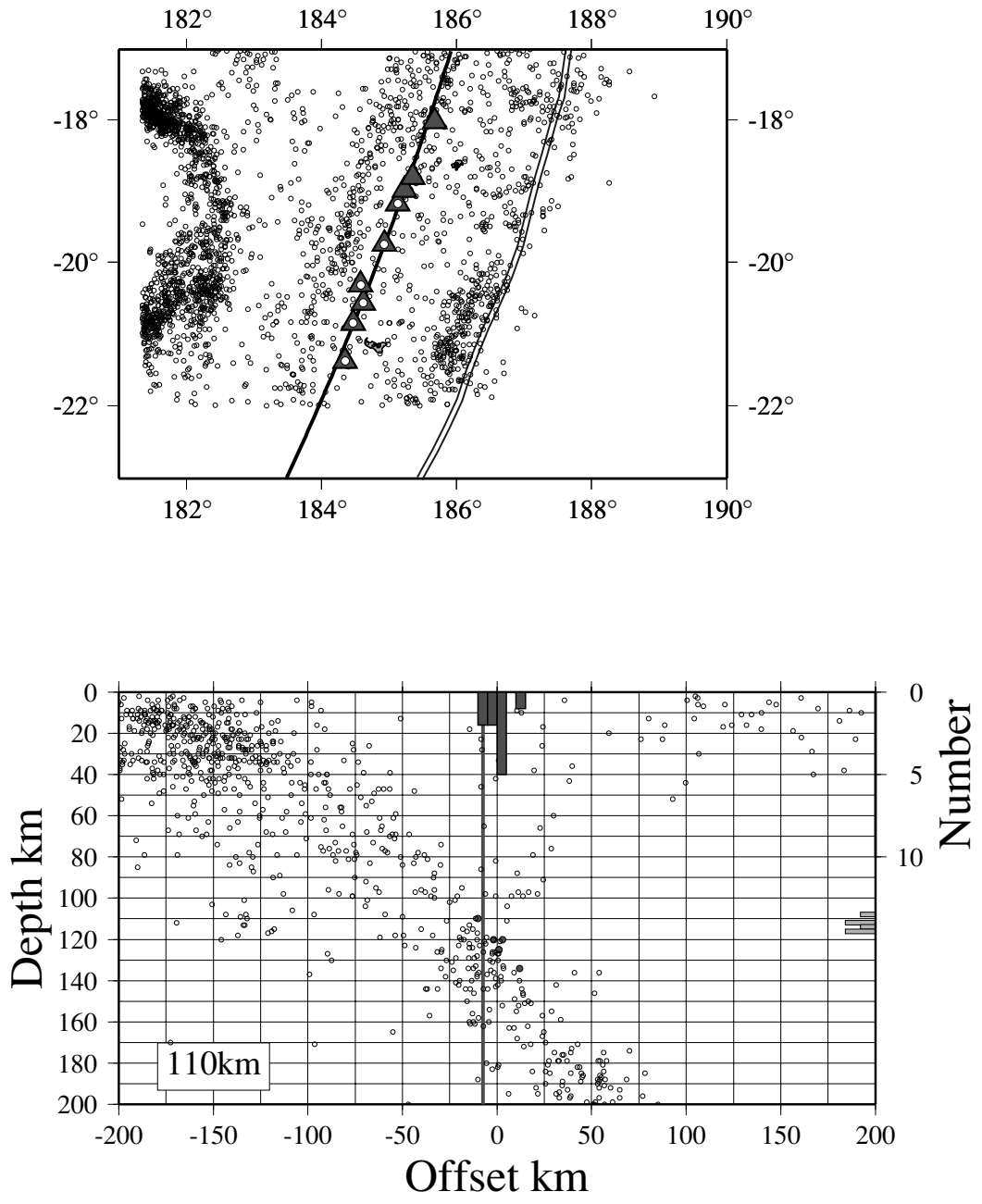

Figure 17. As Fig. 3, for Tonga.

Thus, if the trigger for arc volcanism were the attainment of a critical temperature, T_c, at the interface between the two plates, then the depth at which that temperature is reached would be given by:

$$z \sim \frac{K^2 T_c^2}{\kappa} \frac{V \sin\delta}{Q^2}. \tag{8}$$

Substituting $Q = KT_a/a$, where T_a is the temperature at the base of the plate, and $a \sim \sqrt{\kappa A}$, where A is the age of the ocean floor, gives the condition

$$z' = \frac{z}{V A \sin\delta} = \frac{z}{\phi} \sim \frac{T_c^2}{T_a^2}. \tag{9}$$

Thus, in the absence of dissipative heating, the depth of attainment of a given temperature on the plate boundary should depend on the same combination of quantities contained in the thermal parameter, ϕ.

If, however, there is dissipative heating on the plate boundary, a different parameter describes the depth at which a given temperature is attained. This problem has been addressed by Turcotte & Schubert (1973) and Molnar & England (1990) for the case of two rigid plates sliding past each other, and by Peacock *et al.* (1994) with the added complexity of flow in the mantle wedge. Molnar & England (1990) show that if the shear stress, σ, on the plate boundary were constant

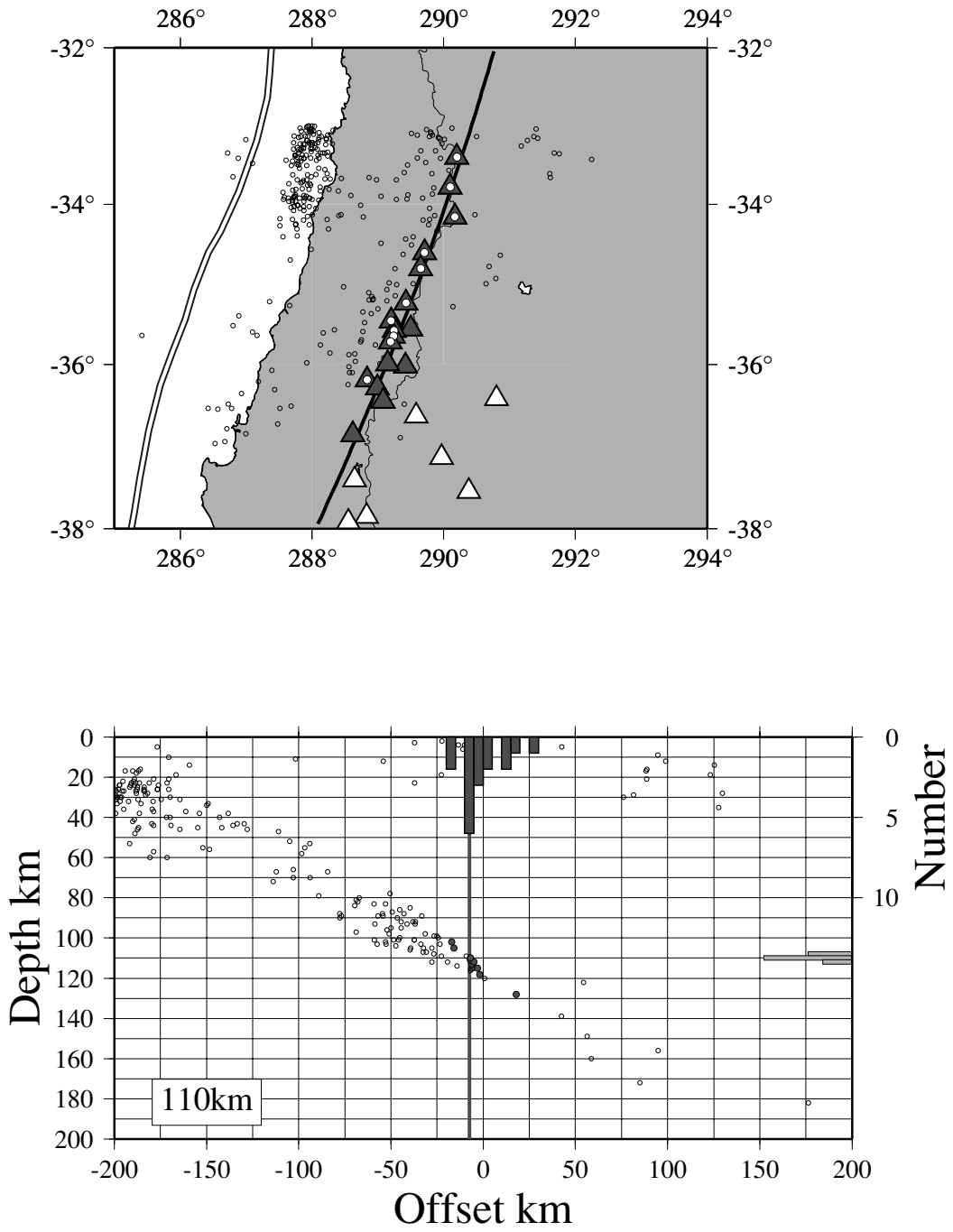

Figure 18. As Fig. 3, for central Chile.

the temperature on the boundary would be given by:

$$T = \frac{(Q + \sigma V)z}{K\left(1 + \sqrt{Vz \sin\delta/\kappa}\right)}. \tag{10}$$

To clarify the dependence, assume that shear heating dominates over the basal heat flux, Q, and that V is large, then

$$T \sim \frac{\sigma V z}{K\sqrt{Vz \sin\delta/\kappa}}. \tag{11}$$

If the trigger for arc volcanism were a critical temperature on the plate boundary, T_c, then (11) shows that the depth z_c at which that temperature is reached would be given by:

$$z_c \sim \frac{\sin\delta}{V\kappa}\left(\frac{K T_c}{\sigma}\right)^2, \tag{12}$$

and (assuming constancy of K, T_c, σ, and κ) D would then be expected to depend upon $(\sin\delta/V)$. If, however, the stress were to depend on depth as $\sigma = \mu\, z$ where μ is a constant, D would be expected to depend upon $(\sin\delta/V)^{\frac{1}{3}}$ [this result is obtained by

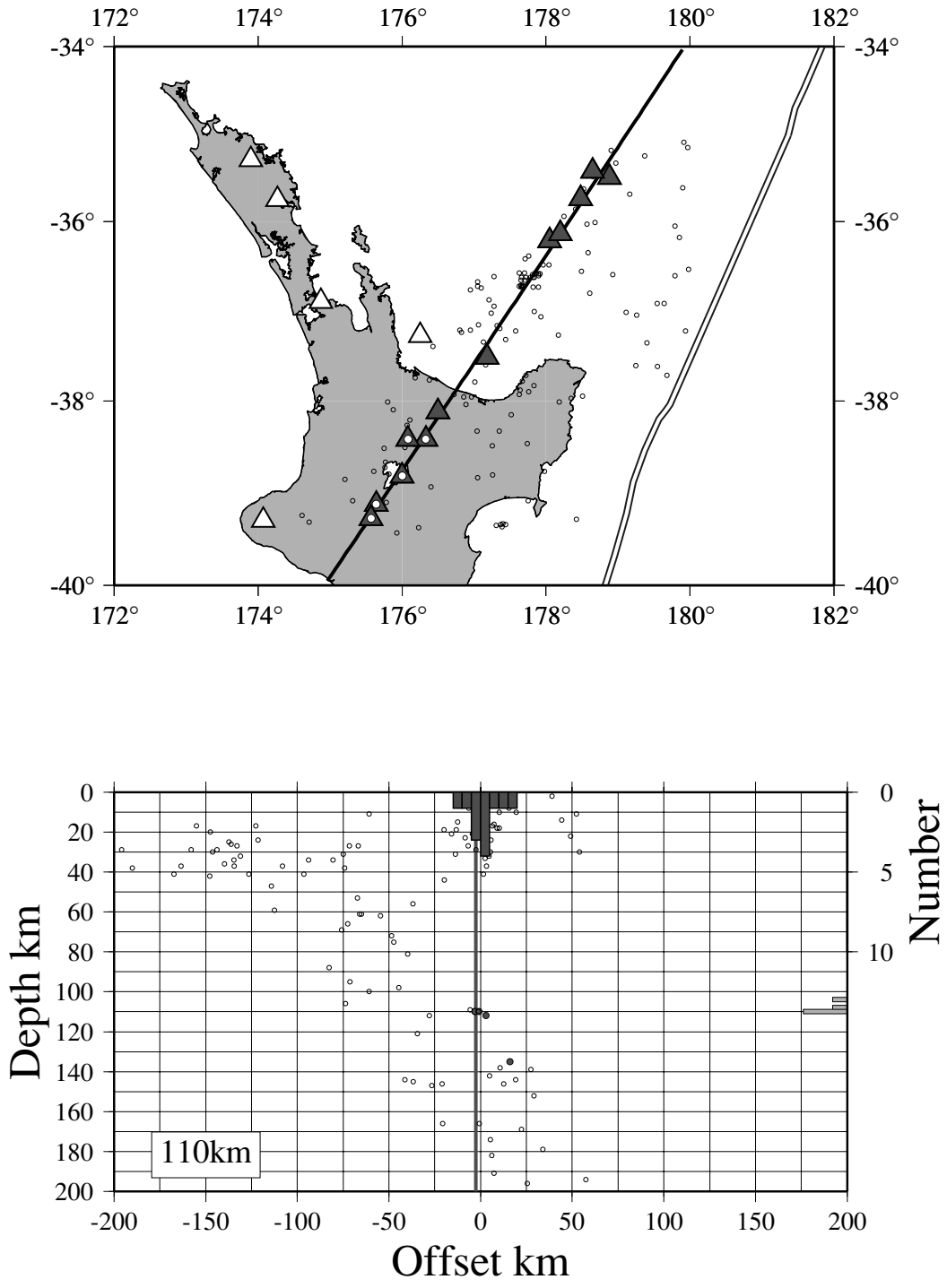

Figure 19. As Fig. 3, for the north of New Zealand.

replacing σ with μz in (10) to (12)]. In Fig. 29(e) we plot D against $\sin \delta/V$; apart from a distortion of the horizontal scale, this figure also illustrates the relation between D and $(\sin \delta/V)^{\frac{1}{3}}$.

When the top of the slab is in contact with the wedge of mantle, circulation in the wedge advects heat towards the top of the slab (e.g. McKenzie 1969; Davies & Stevenson 1992 and see Fig. 1). England & Wilkins (2003) give approximate analytical solutions to the advection and diffusion of heat in slab and overlying wedge, assuming circulation in the wedge approximates to a Newtonian corner flow (e.g. McKenzie 1969). They show that temperatures both near the top of the slab and in the wedge are determined by the balance between the advection and diffusion of heat in the direction perpendicular to the slab. Under these conditions, the characteristic length scale in (1) is the width, $r\delta$, of the wedge at a radial distance r

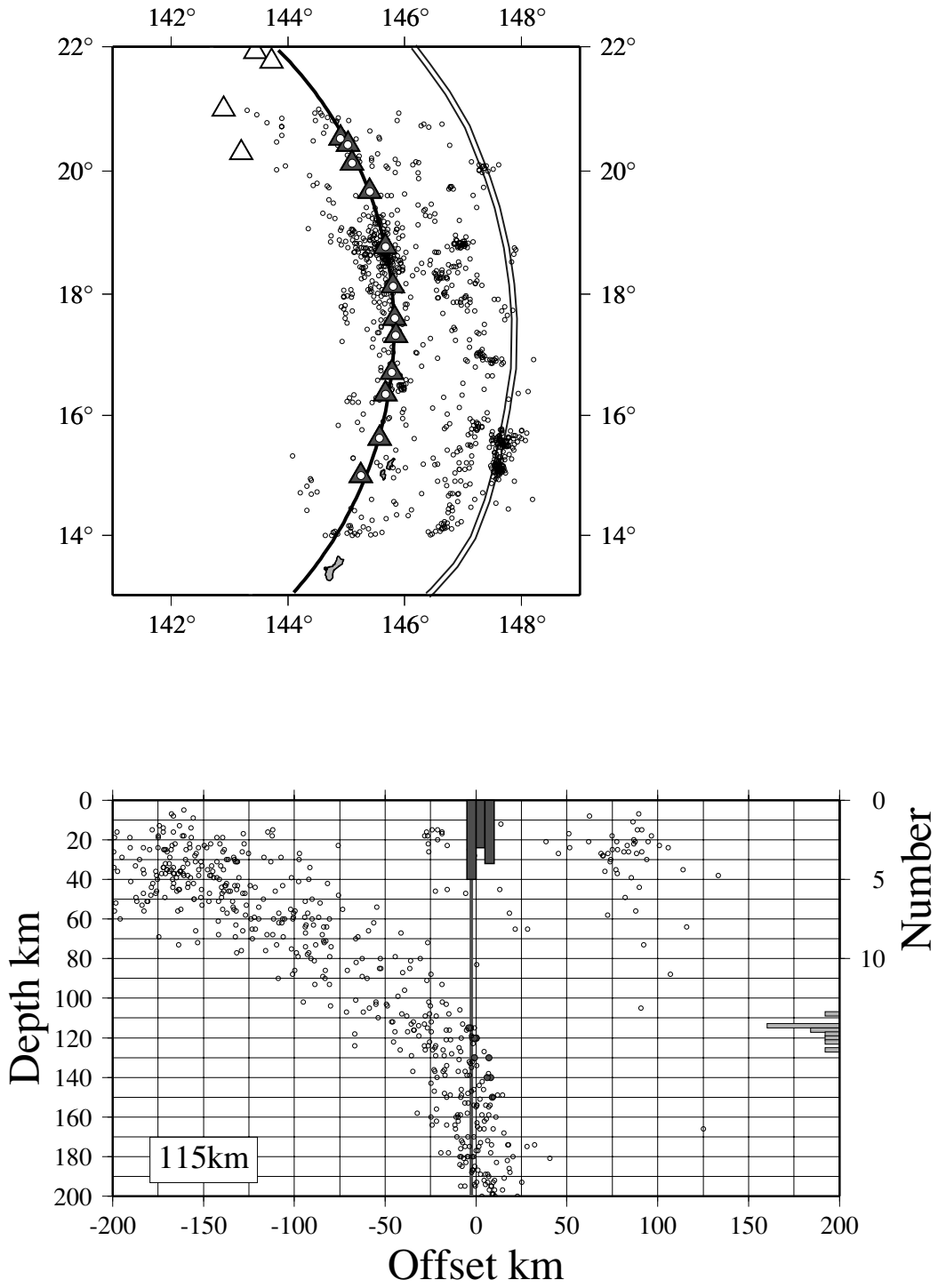

Figure 20. As Fig. 3, for the Marianas arc.

from the wedge corner, and the characteristic speed is the maximum of the velocity component perpendicular to the slab, which scales as $V\delta$, and temperatures depend upon a dimensionless distance of the form

$$z' = \frac{Vr\delta^2}{\kappa}. \tag{13}$$

But $r = (z - z_w)/\sin(\delta)$ where z is depth, and z_w is the depth to the corner of the wedge (Fig. 1), so we may write:

$$z' \sim \frac{V(z - z_w)\delta}{\kappa}. \tag{14}$$

Thus, if the trigger for arc volcanism were a critical temperature on the interface between slab and wedge, or within the wedge itself,

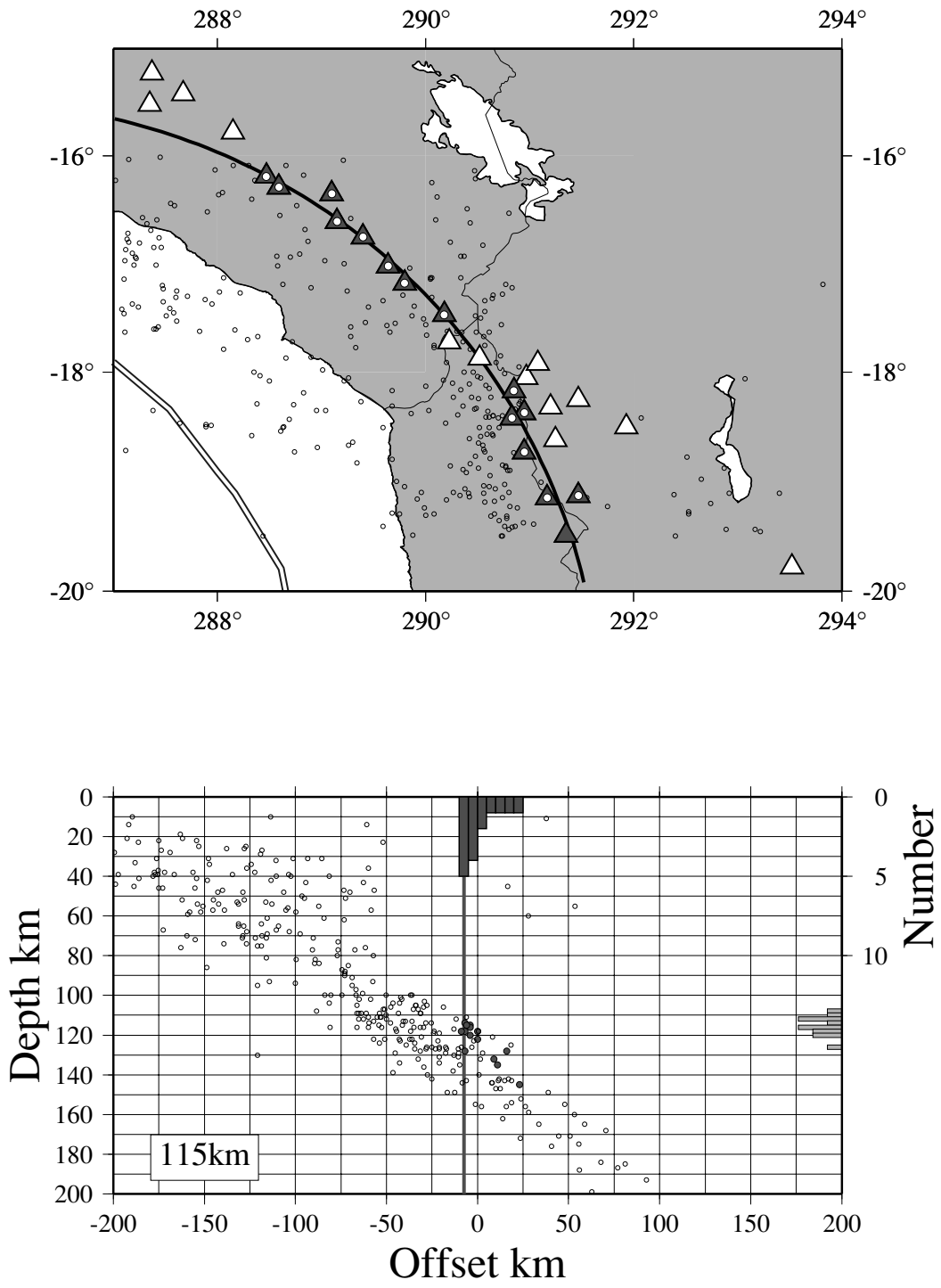

Figure 21. As Fig. 3, for the southern Peru and northern Chile.

we should expect D to vary inversely with V sin δ; this relation is investigated in Fig. 29(f).

In Section 3.3 we analyse the correlations displayed in Fig. 29, but first we return to the question of how backarc spreading rates influence those correlations.

3.2 Influence of backarc spreading rates

Figs 29(c)–(f) plot the depth D against various combinations of subduction parameters that all depend on the plate convergence rate, V. In these plots, the arcs of Tonga, Kermadec, and the Marianas, all of which have significant rates of backarc spreading, are represented by grey symbols when V is calculated from the convergence rates of the major plates alone, and by open symbols when V includes the rate of backarc spreading. It is, at first sight, surprising to note that the grey symbols (for which the rate of backarc spreading is excluded) plot within the trends followed by the other arcs whereas, if the rate of backarc spreading is included, these arcs plot significantly to the right of the trends (open symbols). This observation is, however, explicable if we consider how the increased convergence rate caused

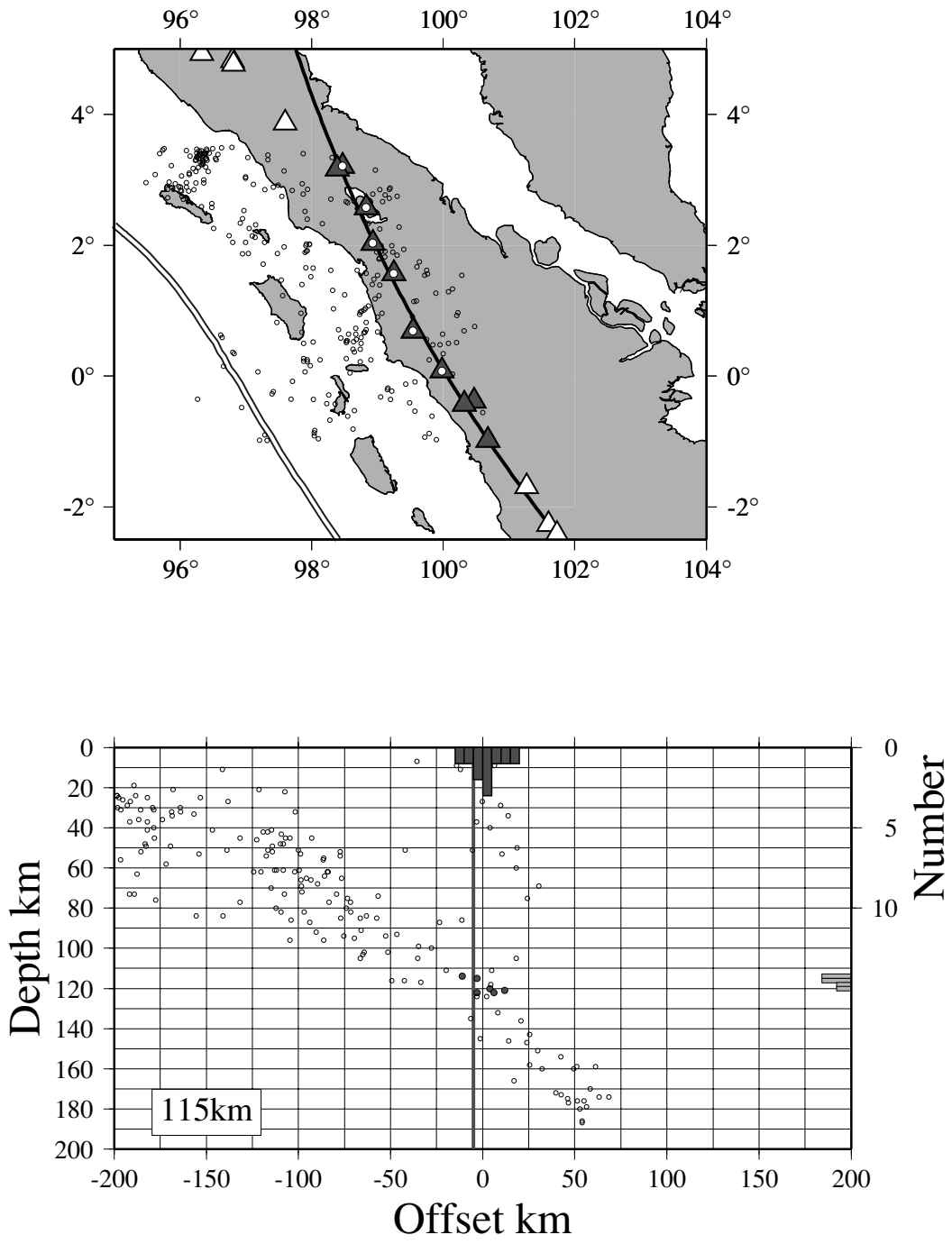

Figure 22. As Fig. 3, for northern Sumatra.

by backarc spreading is related to the transport of heat in the wedge of mantle between slab and overriding plate.

It seems probable that temperature in the upper mantle beneath the volcanoes is strongly influenced by the advection of heat by circulation in the wedge (e.g. Davies & Stevenson 1992; England & Wilkins 2003). In the subduction zones without backarc spreading, all the circulation is directed to and from the wedge corner (Fig. 1), thus carrying heat beneath the arcs. Backarc spreading increases the total intensity of circulation in the wedge, but only a portion of this circulation is directed towards the wedge corner, with the rest being diverted towards the spreading centre (see Ribe 1989). Ribe's study addresses only the form of the circulation in the wedge; we know of no systematic analysis of the attendant heat transfer, but it is plausible to suppose that most of the extra heat advected as a result of backarc spreading is diverted to the spreading centre, rather than contributing extra heat to the arc. If this suggestion is correct, then we might expect the amount of heat advected towards the arc in a subduction zone with backarc spreading to be comparable to

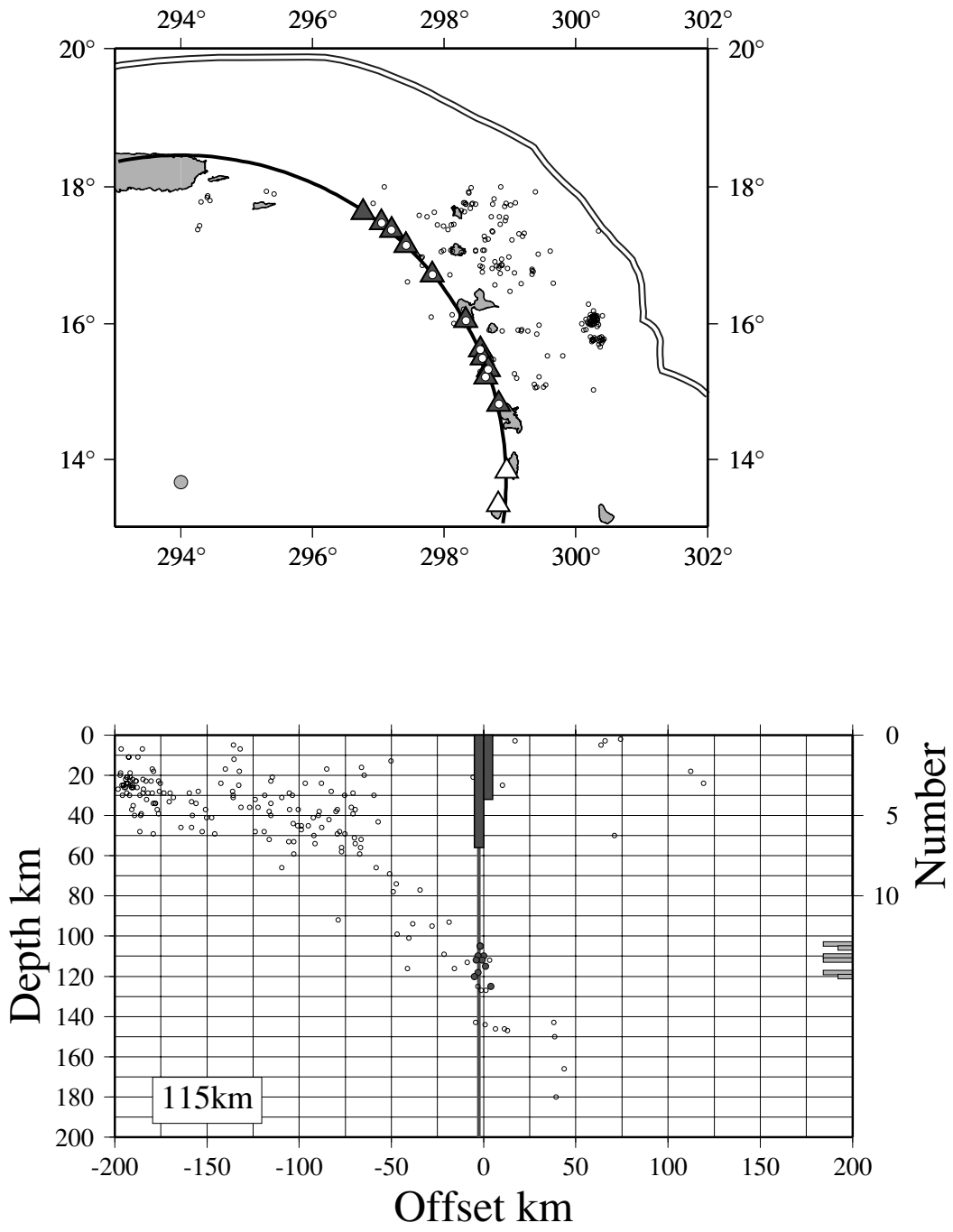

Figure 23. As Fig. 3, for the northern Lesser Antilles.

the amount that would be carried in the absence of spreading. If this were so, then temperatures would scale with the convergence rate excluding the rate of backarc spreading. Our conclusions do not depend on the correctness of this suggestion; the statistical analyses we carry out below exclude the Kermadec, Tonga, and Marianas subduction zones.

3.3 Dependence of depth to top of intermediate-depth seismicity on parameters of subduction

If the process that governs the position of arc volcanoes is described by any of the parameters discussed in Section 3.1, then we might expect to see a correlation between D and that parameter. D need not depend linearly upon the parameter, so we investigate the relations shown in Fig. 29 using the non-parametric Spearman rank-order correlation coefficient (e.g. Press *et al.* 1992). Our conclusions are not sensitive to the measure of correlation employed, and, apart from small quantitative differences, the same results are obtained by using Kendall's τ statistic or, indeed, the linear correlation coefficient. We exclude from our analysis the arcs with significant backarc spreading (Kermadec, Marianas and Tonga) for the reasons discussed in the previous subsection.

The weakest correlation in Fig. 29 is between the depth to the top of the intermediate-depth seismicity, D, and the age of the subducted

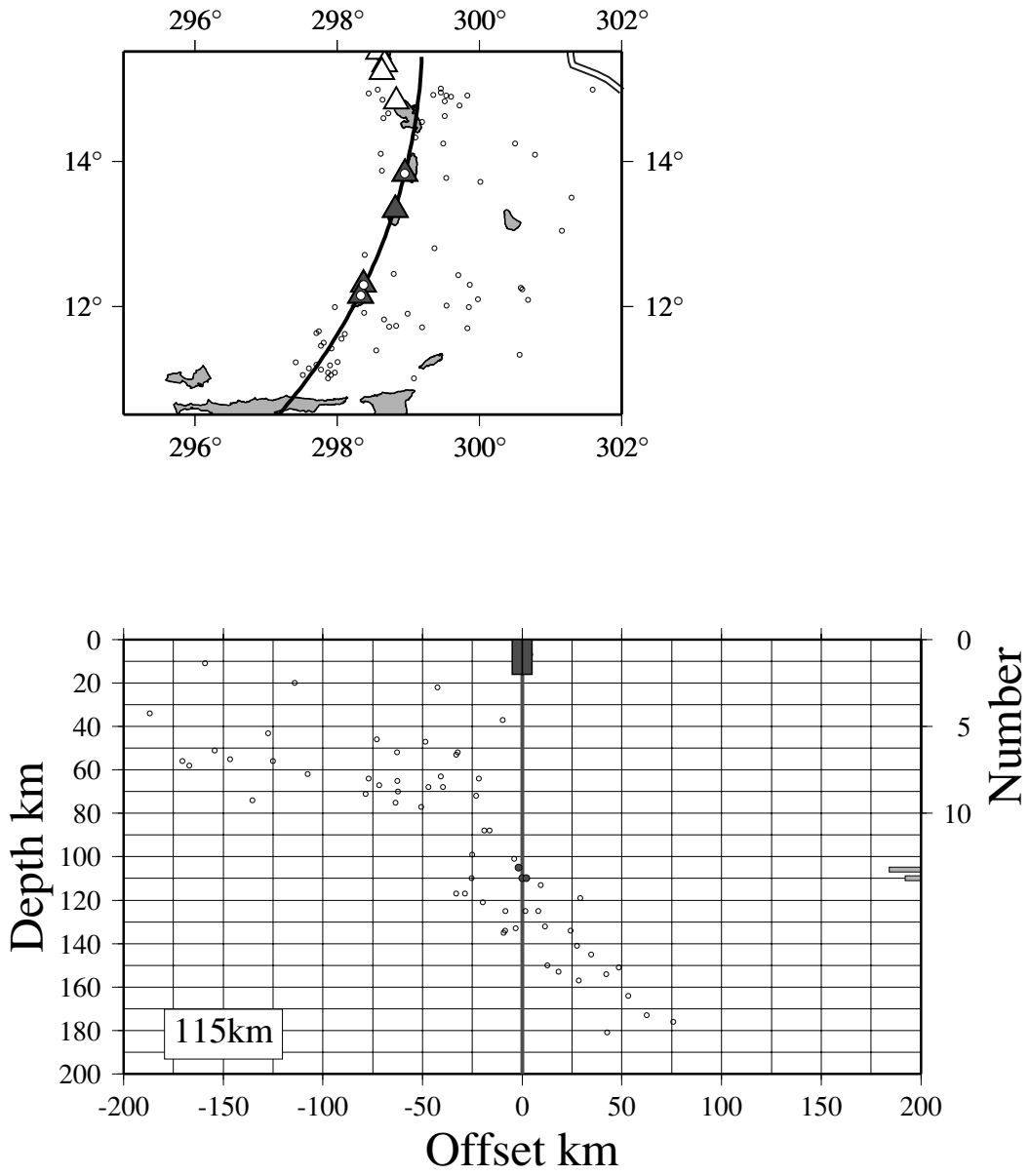

Figure 24. As Fig. 3, for southern Lesser Antilles.

lithosphere (Fig. 29a). The correlation coefficient for these two variables is −0.26 and, for the sample size of 21, this correlation has a 26 per cent probability of having arisen by chance. The dependence of D upon thermal parameter, ϕ [(5), Fig. 29(d)] is also weak; the correlation coefficient is −0.31, with a 16 per cent probability of having arisen by chance. The dependence of D on $\sin(\delta)/V$ [(12), Fig. 29(e)] has a correlation coefficient of 0.33, with a 14 per cent probability of having arisen by chance. Because the rank-order of a set of numbers is not changed by raising them all to the same power, the correlation coefficient between D and $(\sin\delta/V)^{\frac{1}{3}}$ [discussion following (12)] is also 0.33.

The correlations of depth to the top of the intermediate-depth seismicity beneath the volcanoes with slab dip (Fig. 29b) and convergence rate (Fig. 29c) are significant at the 99 per cent level, with correlation coefficients, respectively, of −0.56 and −0.59. The strongest correlation in Fig. 29, however, is between D and $V \sin \delta$ [(14), see Fig. 29f]. The correlation coefficient is −0.85, which has a probability of $\sim 10^{-6}$ of having arisen by chance.

None of the correlations in Figs 29(b), (c) and (f), is likely to have arisen by chance, yet the parameters in these different plots relate to distinctly different aspects of the subduction process. Thus the question arises as to whether there may be other correlations (representing different physical models from those described above) that are equally valid. As with all geological problems, it is possible to invoke enough complexity to preclude analysis, but if we adhere to the simple physical model sketched in Fig. 1, in which heat is advected by the corner flow in the wedge, and diffuses through the wedge and surrounding plates, then there are six

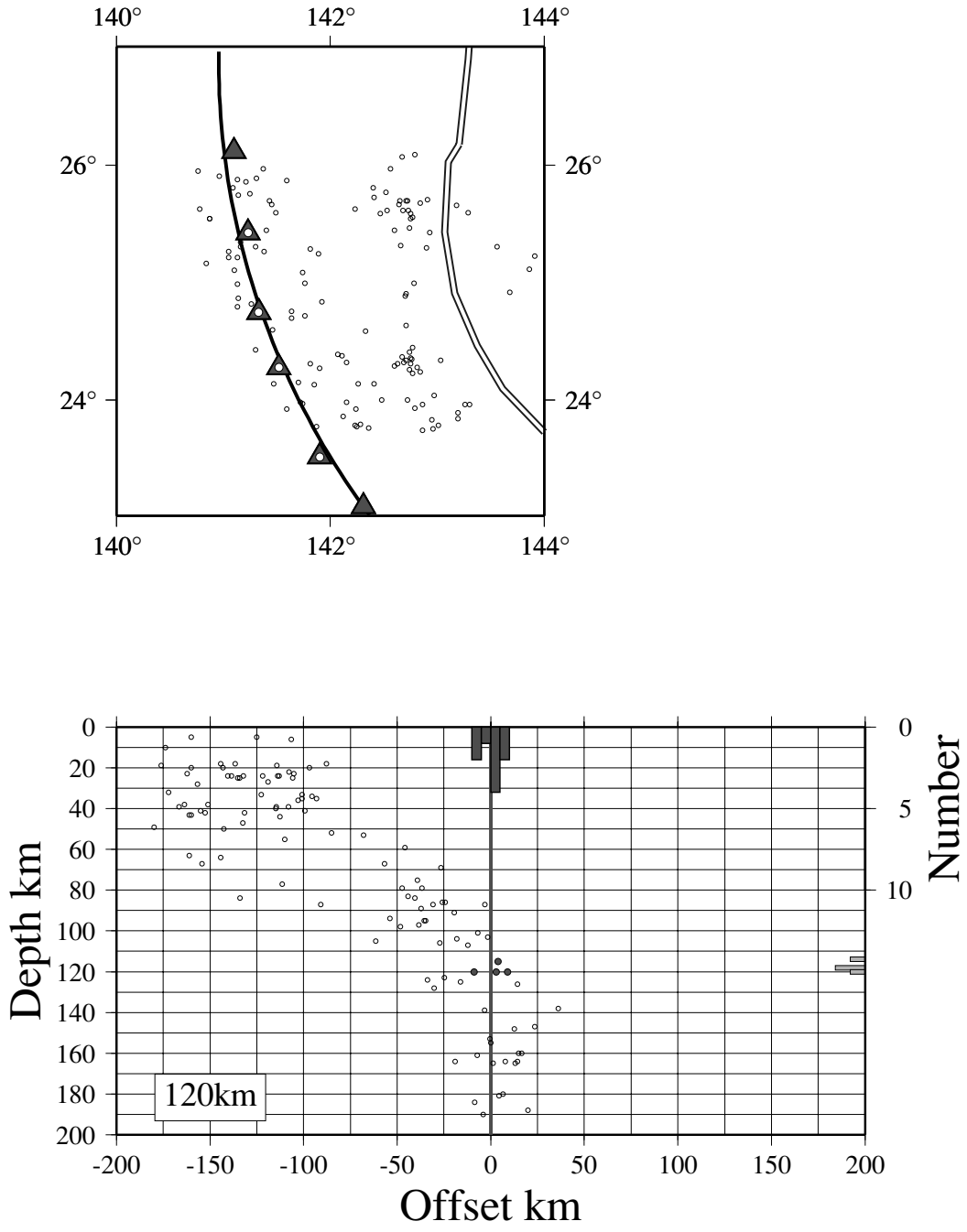

Figure 25. As Fig. 3, for the Bonin arc.

parameters that might influence the thermal structure of subduction zones: the slab thickness, a, its down-dip length, the thickness, z_w, of the overriding plate, the convergence rate, V, and dip, δ, of the slab, and the thermal diffusivity, κ. The temperature structure must be expressible in terms of dimensionless combinations of these parameters.

The parameters V and κ can form a dimensionless combination only when V is multiplied by a length scale and divided by κ (see eq. 1); the remaining possible combinations are ratios of the parameters that have dimensions of length. The dip, being dimensionless, can multiply any of these combinations either as itself or, as we have seen above [e.g. (5), (6), (13)], in a trigonometric function.

The depth, D, to the top of the intermediate-depth seismicity beneath the arcs must be one of the parameters that influence temperature. We now argue that the remaining length parameters appear not to influence the temperature structure in any systematic way. One might expect, if the thickness of the overriding plate influenced the location of the volcanoes, that there would be a clear contrast in D, the depth to the top of the intermediate-depth seismicity,

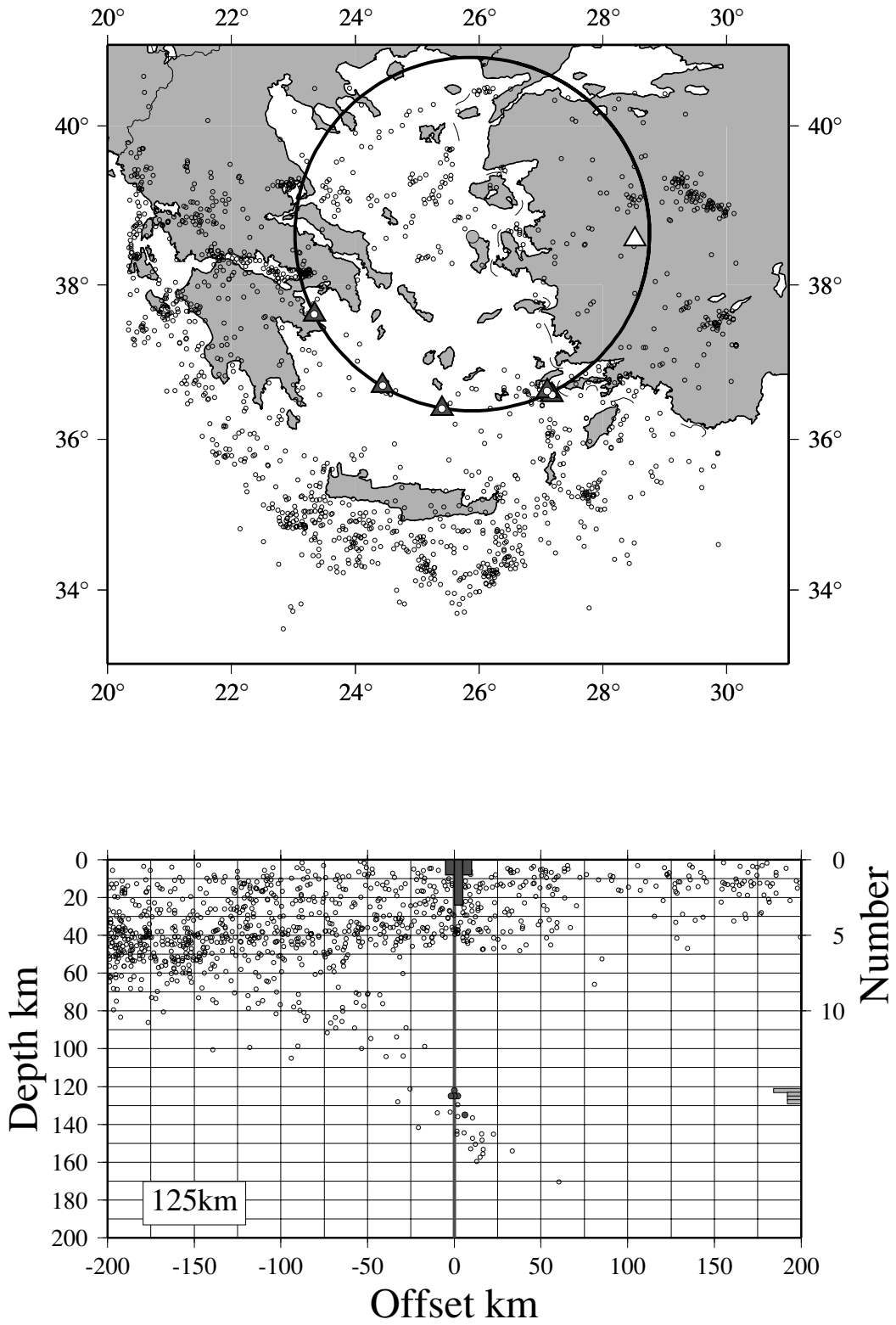

Figure 26. As Fig. 3, for the Aegean.

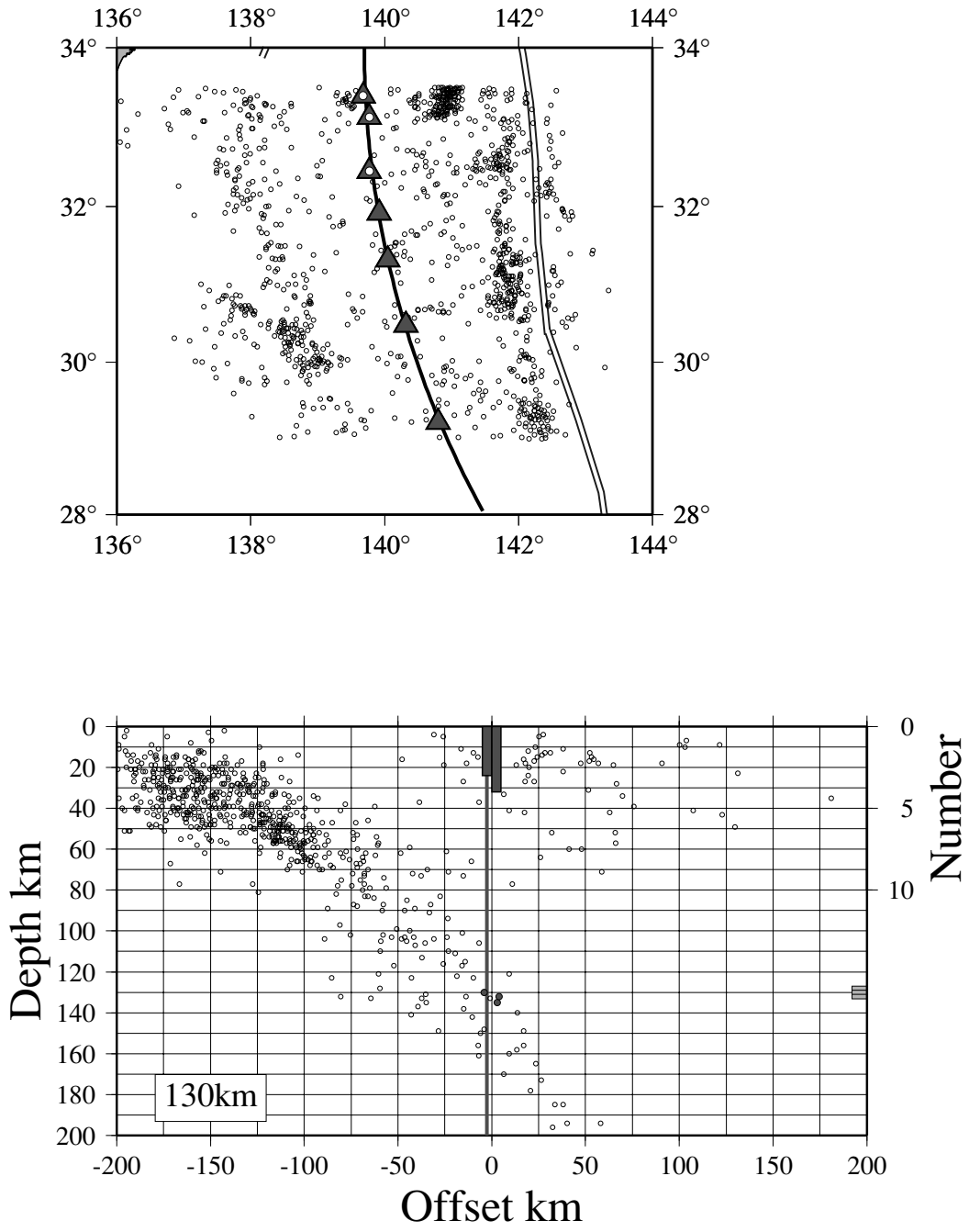

Figure 27. As Fig. 3, for the Izu arc.

between arcs on continental crust and those on oceanic crust; yet arcs on crust of each type are distributed throughout the depth range shown in Table 1. We have already shown that the slab thickness (or, equivalently, its age) is unrelated to D (Fig. 29a). The rank-order correlation coefficient between down-dip length of the slab (Table 1) and D is 0.08 (not illustrated), and thus insignificant.

Because there is no systematic relation between D and any of the other length parameters, we conclude that D is the only length parameter that influences temperatures in subduction zones. We therefore need consider only the single dimensionless parameter:

$$z' = \frac{DV \sin^n \delta}{\kappa}. \tag{15}$$

The powers of D, V, and κ are fixed in this expression, on dimensional grounds; however the dip, or functions of the dip, may appear with any power. Because the dip enters into many of the expressions above as its sine (e.g. 5, 12, 14), we use this quantity rather than δ itself. Over the observed dip range of 30–75°, the difference between δ and sin δ is unimportant in this context.

We calculated the rank-order correlation coefficient between D and $V \sin^n \delta$ using the data of Table 1, excluding arcs with backarc

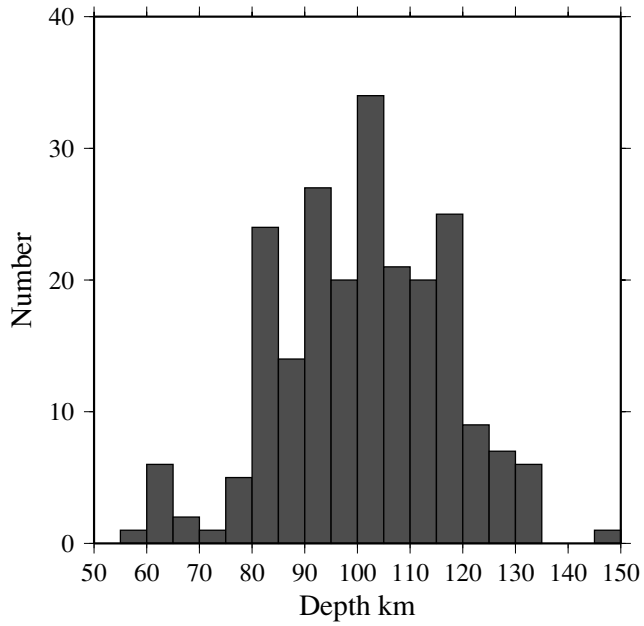

Figure 28. Distribution of depths to the top of the intermediate-depth seismicity beneath individual volcanoes, adjusted to the location of their volcanic fronts (see Figs 3 to 27).

Table 2. Notation.

a	Thickness of the slab
A	Age of slab
K	Coefficient of thermal conductivity
L	Characteristic length
L'	Dimensionless distance UL/κ
Q	Heat flux at the base of the oceanic lithosphere
r	Radial distance from wedge corner (Fig. 1)
T	Temperature
U	Characteristic speed
V	Convergence rate between plates (plate relative velocity resolved perpendicular to the arc; see Sections 3.1, 3.2 for discussion of backarc spreading)
z	Depth below Earth's surface
z_w	Depth of wedge corner beneath Earth's surface (Fig. 1)
δ	Dip of the zone of intermediate-depth seismicity
κ	Thermal diffusivity
ϕ	Thermal parameter $= VA \sin \delta$

spreading. The most significant correlations are found where n is between about 1 and 2 (Fig. 30). All correlations illustrated have negative correlation coefficients. When $n > 0.4$, the correlations have smaller than 10^{-3} probability of arising by chance, and in the range $1 \lesssim n \lesssim 3$ the probability is smaller than 10^{-5}. We take this result to indicate that it is highly likely that the depth, D of the top of the intermediate-depth seismicity beneath volcanoes depends upon both the rate of convergence between the plates, V, and the dip, δ of the slab, and that other dependences – not only those illustrated in Fig. 29, but any dependence that could be suggested within the simple framework of thermal diffusion and advection in the slab and mantle wedge (Fig. 1) – are less likely.

4 CONCLUSION

The analysis given in the previous sections establishes four important conclusions about the relationship between arc volcanoes and their underlying slabs. First, the locations of volcanoes forming the frontal arcs lie within a few kilometres of small circles (Table 1, see also Tovish & Schubert (1978)). Secondly, the depth to the top of the intermediate-depth seismicity beneath these small circles is also constant to within a few kilometres along individual arc segments (Figs 3 to 27). Thirdly, these depths vary, from arc to arc, between about 65 km and 130 km. Finally, the depths increase systematically with a quantity that is closely related to the descent speed of the slab (Figs 29f and 30). These conclusions make it reasonable to infer that, among all the processes that occur beneath island arcs, there is a single process that dictates the location of the volcanoes.

We may go further, and rule out some of the models that are commonly believed to explain the location of arc volcanism. For example, it might seem reasonable to expect that the younger the ocean floor entering the subduction zone, the higher would be the geothermal gradients, and therefore the conditions necessary to promote melting would be achieved at shallower depths. The observations rule out any strong dependence of the location of arc volcanism with the age of the oceanic lithosphere (Figs 29a and d). We therefore conclude that, although the thermal structure of the oceanic lithosphere may be important in particular cases (perhaps when slab of close to zero age is being subducted (e.g. Defant & Drummond 1990)), slab age is not generally an important factor in controlling the locus of arc volcanism.

As another example, a common view is that the arc volcanoes all lie above places where the slabs attain a roughly constant depth of about 110 km, and this relation is explained by proposing that volcanism is triggered by the release of H_2O by the dehydration of amphibole or chlorite at roughly constant pressures around 3.5 GPa (see, e.g. review by Tatsumi & Eggins 1995, and references therein). Figs 3 to 27 show that the depth to the slab beneath the volcanoes varies, from place to place, by almost a factor of two; this observation cannot be reconciled in a simple way with a trigger that is pulled when the top of the slab reaches a constant depth.

Recognizing that there is variation in the depths of the slab beneath arc volcanoes, Davies & Stevenson (1992) proposed a mechanism of fluid release followed by steps of upward percolation, and lateral transport within the flow of the wedge. This mechanism now seems implausible in view of the evidence that fluid from the slab reaches the arc volcanoes within a few tens of thousands of years (e.g. Hawkesworth *et al.* 1997; Turner *et al.* 2000), whereas lateral transport within the wedge would require time-scales of order a million years [the range in depths to the slab is ∼60 km and rates of vertical motion of the slab and overlying wedge are tens of kilometres per million years (Table 1)]. Furthermore, the relationship predicted by Davies & Stevenson (1992) between dip of the slab and its depth beneath the volcanoes is not observed (Fig. 29b). We therefore conclude that, although it is inescapable that fluid released from the slab must be involved in the melting of the wedge beneath arc volcanoes, the locations of the volcanoes cannot be explained simply by the release of that fluid in a single pressure-dependent dehydration reaction (see, e.g. Schmidt & Poli 1998).

The strongest correlation between depth, D, to the top of the intermediate-depth seismicity and subduction zone parameters is with the descent speed, $V \sin \delta$, of the slab (Figs 29f and 30). If the wedge is mechanically coupled to the slab, then we should expect that increasing convergence rate should raise the rate at which hot

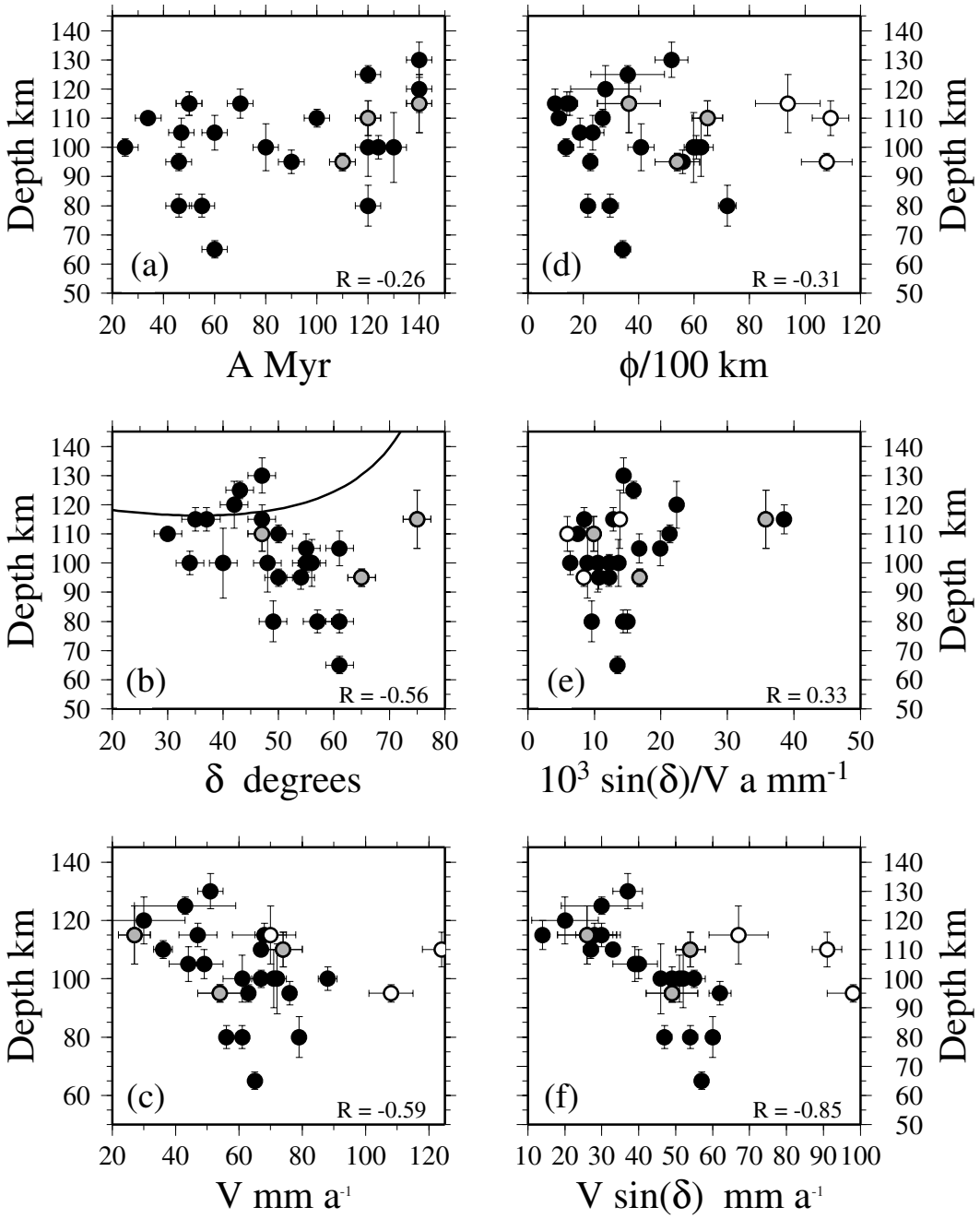

Figure 29. The depth, D, to the top of the intermediate-depth seismicity beneath volcanic arcs plotted against different subduction parameters; data from Table 1. In each plot, the arcs with significant backarc spreading are distinguished by grey symbols; in (c–f), where convergence rate, V, is contained in the parameter, these arcs are also shown by an open symbol, representing the value of the parameter calculated by including the backarc spreading rate in V. The Spearman rank-order correlation coefficient, R, between D and the relevant parameter is shown at the bottom right of each panel. (a) D against age of the ocean floor entering the trench; (b) D against dip, δ, of the zone of intermediate-depth seismicity; the solid line shows the relation between D and δ predicted by Davies & Stevenson (1992). (c) D against plate convergence rate, V; (d) D against the thermal parameter, ϕ (5); (e) D against $\sin(\delta)/V$; (f) D against the descent speed of the slab ($V \sin\delta$). Error bars in panels (a) to (c) indicate ranges in the observed quantities; the dip is taken to be uncertain by 2.5°, and ages are assigned an uncertainty of 5 Myr. These ranges in observation are propagated, as though they were statistical uncertainties, to yield the error bars in panels (d) to (f).

mantle is drawn towards the wedge corner (e.g. Davies & Stevenson 1992; Peacock *et al.* 1994). Approximate analytical solutions to this problem, given by England & Wilkins (2003), suggest that temperatures in the wedge scale with the descent rate of the slab (see eq. 14). Thus calculations of the thermal structure of subduction zones imply that the depth at which a given isotherm is found will vary inversely with the descent rate of the slab.

The observations of Fig. 29(f) show that the depth to the slab beneath arc volcanoes correlates strongly and negatively with the descent speed of the slab, and the discussion surrounding Fig. 30 shows that no stronger correlation exists within the simple framework analysed here. We therefore conclude that the locations of the arc volcanoes are governed by a process occurring at a critical temperature rather than at a critical pressure. Without a review of

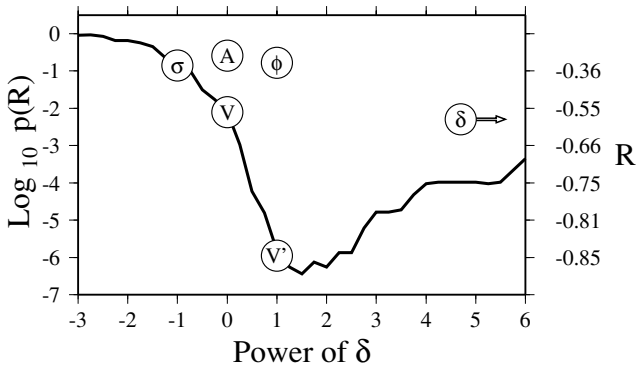

Figure 30. Values (R) and significance ($p(R)$) of the Spearman rank-order correlation coefficient between D and $\sin^n\delta$ for the subduction parameters listed in Table 1, plotted against n. Right-hand axis gives values of the correlation coefficient; left-hand axis shows (logarithmically) the probability that a correlation coefficient of that magnitude could have arisen by chance from a sample of the size of Table 1 (21, excluding arcs with backarc spreading). Symbols in circles refer to the correlations illustrated in Fig. 29. A: age (Fig. 29a); V: convergence rate; the correlation for δ (dip, Fig. 29b) plots off the right of the figure (Fig. 29c); ϕ: thermal parameter (Fig. 29d); σ indicates correlation of D with $\sin(\delta)/V$, suggested by (12) (Fig. 29e); $V'(=V\sin\delta)$: descent speed of the slab (Fig. 29f).

petrological data and ideas, which is beyond the scope of this paper, it is not possible to determine what this process is. Any petrological model of the genesis of arc volcanism should, however, be constrained by the simple relation displayed in the observations presented here.

ACKNOWLEDGMENTS

We have benefited from many discussions with Peter Molnar. Geoffrey Abers and Stephen Kirby gave many helpful comments. We are also grateful to Molnar and Hannah England for their help in the production of Figs 3 to 27. This work was supported by the Natural Environment Research Council.

REFERENCES

Abers, G.A., 1992. Relationship between shallow- and intermediate-depth seismicity in the eastern Aleutian subduction zone, *Geophys. Res. Lett.,* **19,** 2019–2022.

Bevis, M. & Isacks, B., 1984. Hypocentral trend-surface analysis: Probing the geometry of Benioff zones, *J. geophys. Res.,* **89,** 6153–6170.

Bevis, M. *et al.*, 1995. Geodetic observations of very rapid convergence and back-arc extension at the Tonga arc, *Nature,* **374,** 249–251.

Davies, H. & Stevenson, D., 1992. Physical model of the source region of subduction volcanics, *J. geophys. Res.,* **97,** 2037–2020.

Defant, M.J. & Drummond, M.S., 1990. Derivation of some modern arc magmas by melting of young subducted lithosphere, *Nature,* **347,** 662–665.

DeMets, C., Gordon, R., Argus, D. & Stein, S., 1994. The effect of recent revisions to the geomagnetic reversal time scale on estimates of current plate motions, *Geophys. Res. Lett.,* **21,** 2191–2194.

DeMets, C., Jansma, P., Mattioli, G., Dixon, T., Farina, F., Bilham, R., Calais, E. & Mann, P., 2000. GPS geodetic constraints on Caribbean-North America plate motion, *Geophys. Res. Lett.,* **21,** 2191–2194.

Engdahl, E. & Gubbins, D., 1987. Simultaneous travel time inversion for earthquake location and subduction zone structure in the central Aleutian islands, *J. geophys. Res.,* **92,** 13 855–13 862.

Engdahl, E., Dewey, J.W. & Fujita, K., 1982. Earthquake location in island arcs, *Phys. Earth planet. Inter.,* **30,** 145–156.

Engdahl, E., van der Hilst, R. & Buland, R., 1998. Global teleseismic earthquake relocation with improved travel times and procedures for depth determination, *Bull. seism. Soc. Am.,* **88,** 722–743.

England, P. & Wilkins, C., 2003. A simple analytical approximation to the temperature structure in subduction zones, *Geophys. J. Int.,* submitted.

Fujita, E., Engdahl, K. & Sleep, N.H., 1981. Subduction zone calibration and teleseismic relocation of thrust zone events in the central Aleutian islands, *Bull. seism. Soc. Am.,* **71,** 1805–1828.

Gill, J., 1981. *Orogenic Andesites and Plate Tectonics*, Springer-Verlag, New York.

Hawkesworth, C.J., Turner, S.P., McDermott, F., Peate, D.W. & van Calsteren, P., 1997. U-Th isotopes in arc magmas: Implications for element transfer from the subduceted crust, *Science,* **276,** 551–555.

Helffrich, G. & Abers, G.A., 1997. Slab low-velocity layer in the eastern Aleutian subduction zone, *Geophys. J. Int.,* **130,** 640–648.

Igarishi, T., Matsuzawa, T., Umino, N. & Hasegawa, A., 2001. Spatial distribution of focal mechnisms for interplate and intraplate earthquakes associated with the subducting Pacific plate beneath the northeastern Japan arc: A triple-planed deep sesimic zone, *J. geophys. Res.,* **106,** 2177–2191.

Isaacs, B.L. & Molnar, P., 1971. Distribution of stresses in the descending lithosphere from a global survey of focal mechanism solutions of mantle earthquakes, *Rev. Geophys.,* **9,** 103–174.

Jarrard, R.D., 1986. Relations among subduction parameters, *Rev. Geophys.,* **24,** 217–284.

Kirby, S., Durham, W.B. & Stern, L., 1991. Mantle phase changes and deep-earthquake faulting in subduction lithosphere, *Science,* **252,** 216–225.

Le Pichon, X., Chamot-Rooke, N., Lallemant, S., Noomen, R. & Veis, G., 1995. Geodetic determination of the kinematics of central Greece with respect to Europe: Implications for Eastern Mediterranean tectonics, *J. geophys. Res.,* **100,** 12 675–12 690.

McKenzie, D., 1969. Speculations on the consequences and causes of plate motion, *Geophys. J. R. astr. Soc.,* **18,** 1–32.

Molnar, P. & England, P., 1990. Temperatures, heat flux, and frictional stress near major thrust faults, *J. geophys. Res.,* **95,** 4833–4856.

Molnar, P., Freedman, D. & Shih, J., 1979. Lengths of intermediate and deep seismic zones and temperatures in downgoing slabs of lithosphere., *Geophys. J. R. astr. Soc.,* **56,** 41–54.

Mueller, R.D., Roest, W.R., Royer, J.-Y., Gahagan, L.M. & Scalter, J.G., 1997. Digital isochrons of the world oceans, *J. geophys. Res.,* **102,** 3211–3214.

Parsons, B. & Sclater, J.G., 1978. An analysis of the variation of ocean floor bathymetry and heat flow with age, *J. geophys. Res.,* **83,** 803–827.

Peacock, S.M., Rushmer, T. & Thompson, A.B., 1994. Partial melting of subducting oceanic crust, *Earth planet. Sci. Lett.,* **121,** 227–244.

Press, W., Teukolsky, S., Vetterling, W. & Flannery, B., 1992. *Numerical Recipes: The Art of Scientific Computing,* 2nd edn, Cambridge University Press, Cambridge.

Ribe, N., 1989. Mantle flow induced by back arc spreading, *Geophys. J. Int.,*, **98,** 85–91.

Schmidt, M.W. & Poli, S., 1998. Experimentally based water budgets for dehydrating slabs and consequences for arc magma generation, *Earth planet. Sci. Lett.,* **163,** 361–379.

Seno, T., Stein, S. & Gripp, A., 1993. A model for the motion of the Philippine plate consistent with NUVEL1 and geological data, *J. geophys. Res.,*, **98,** 17 941–17 948.

Siebert, L. & Simkin, T., 2002. Volcanoes of the world: an illustrated catalog of Holocene volcanoes and their eruptions., Smithsonian Institution Digital Information Series GVP-3., http://www.volcano.si.edu/gvp/world.

Tatsumi, Y., 1986. Formation of the volcanic front in subduction zones, *Geophys. Res. Lett.,* 717–720.

Tatsumi, Y. & Eggins, S., 1995. *Subduction Zone Magmatism, Blackwell Science*, Cambridge, MA.

Tovish, A. & Schubert, G., 1978. Island arc curvature, velocity of convergence and angle of subduction, *Geophys. Res. Lett.,* **5,** 329–332.

Turcotte, D.L. & Schubert, G., 1973. Frictional heating of descending lithosphere, *J. geophys. Res.,* **78,** 5876–5886.

Turner, S., George, R.M.M., Evans, P.J., Hawkesworth, C.J. & Zellmer, G.F., 2000. Time-scales of magma formation, ascent, and storage

beneath subduction-zone volcanoes, *Phil. Trans. R. Soc. Lond. Ser. A,* **358,** 1443–1464.

Wessel, P. & Smith, W., 1995. New version of the Generic Mapping Tools released, *EOS, Trans. Am. geophys. Un.,* **76,** 329.

Zhao, D., Hasegawa, A. & Kanamori, H., 1994. Deep structure of Japan subduction zone as derived from local, regional, and teleseismic events, *J. geophys. Res.,* **99,** 22 313–22 330.

Zhao, D., Matsuzawa, T. & Hasegawa, A., 1997. Morphology of the subducting slab boundary in the northeastern Japan arc, *Phys. Earth planet. Inter.,* **102,** 89–104.